


TECH BRIEFS

NATIONAL AERONAUTICS AND SPACE ADMINISTRATION

-  Technology Focus
-  Electronics/Computers
-  Software
-  Materials
-  Mechanics/Machinery
-  Manufacturing
-  Bio-Medical
-  Physical Sciences
-  Information Sciences
-  Books and Reports

INTRODUCTION

Tech Briefs are short announcements of innovations originating from research and development activities of the National Aeronautics and Space Administration. They emphasize information considered likely to be transferable across industrial, regional, or disciplinary lines and are issued to encourage commercial application.

Availability of NASA Tech Briefs and TSPs

Requests for individual Tech Briefs or for Technical Support Packages (TSPs) announced herein should be addressed to

National Technology Transfer Center

Telephone No. **(800) 678-6882** or via World Wide Web at **www.nttc.edu**

Please reference the control numbers appearing at the end of each Tech Brief. Information on NASA's Innovative Partnerships Program (IPP), its documents, and services is also available at the same facility or on the World Wide Web at **<http://www.nasa.gov/offices/ipp/network/index.html>**

Innovative Partnerships Offices are located at NASA field centers to provide technology-transfer access to industrial users. Inquiries can be made by contacting NASA field centers listed below.

Ames Research Center
Lisa L. Lockyer
(650) 604-1754
lisa.l.lockyer@nasa.gov

Dryden Flight Research Center
Yvonne D. Gibbs
(661) 276-3720
yvonne.d.gibbs@nasa.gov

Glenn Research Center
Kathy Needham
(216) 433-2802
kathleen.k.needham@nasa.gov

Goddard Space Flight Center
Nona Cheeks
(301) 286-5810
nona.k.cheeks@nasa.gov

Jet Propulsion Laboratory
Andrew Gray
(818) 354-4906
gray@jpl.nasa.gov

Johnson Space Center
information
(281) 483-3809
jsc.techtran@mail.nasa.gov

Kennedy Space Center
David R. Makufka
(321) 867-6227
david.r.makufka@nasa.gov

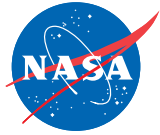
Langley Research Center
Elizabeth B. Plentovich
(757) 864-2857
elizabeth.b.plentovich@nasa.gov

Marshall Space Flight Center
Jim Dowdy
(256) 544-7604
jim.dowdy@msfc.nasa.gov

Stennis Space Center
Ramona Travis
(228) 688-3832
ramona.e.travis@nasa.gov

Carl Ray, Program Executive
Small Business Innovation
Research (SBIR) & Small
Business Technology
Transfer (STTR) Programs
(202) 358-4652
carl.g.ray@nasa.gov

Doug Comstock, Director
Innovative Partnerships
Program Office
(202) 358-2221
doug.comstock@nasa.gov



TECH BRIEFS

NATIONAL AERONAUTICS AND SPACE ADMINISTRATION



5 Technology Focus: Data Acquisition

- 5 Portable Handheld Optical Window Inspection Device
- 5 Saliency Assignment for Multiple-Instance Data and Its Application to Crop Yield Prediction
- 6 Speech Acquisition and Automatic Speech Recognition for Integrated Spacesuit Audio Systems
- 6 Predicting Long-Range Traversability From Short-Range Stereo-Derived Geometry
- 7 Browser-Based Application for Telemetry Monitoring of Robotic Assets



9 Electronics/Computers

- 9 Miniature Low-Noise G-Band I-Q Receiver
- 9 Methods of Using a Magnetic Field Response Sensor Within Closed, Electrically Conductive Containers
- 10 Differential Resonant Ring YIG Tuned Oscillator



13 Manufacturing & Prototyping

- 13 Microfabricated Segmented-Involute-Foil Regenerator for Stirling Engines
- 13 Reducing Seal Adhesion in Low Impact Docking Systems
- 14 Optimal Flow Control Design
- 14 Corrosion-Resistant Container for Molten-Material Processing



17 Mechanics/Machinery

- 17 Reusable Hot-Wire Cable Cutter
- 17 Deployment of a Curved Truss
- 18 High-Volume Airborne Fluids Handling Technologies To Fight Wildfires



21 Materials

- 21 Modeling of Alkane Oxidation Using Constituents and Species
- 21 Fabrication of Lanthanum Telluride 14-1-11 Zintl High-Temperature Thermoelectric Couple
- 22 A Computer Model for Analyzing Volatile Removal Assembly



23 Physical Sciences

- 23 Analysis of Nozzle Jet Plume Effects on Sonic Boom Signature
- 24 Optical Sidebands Multiplier
- 24 Single Spatial-Mode Room-Temperature-Operated 3.0 to 3.4 μm Diode Lasers
- 24 Self-Nulling Beam Combiner Using No External Phase Inverter
- 25 Portable Dew Point Mass Spectrometry System for Real-Time Gas and Moisture Analysis
- 25 Maximum Likelihood Time-of-Arrival Estimation of Optical Pulses via Photon-Counting Photodetectors
- 26 Handheld White Light Interferometer for Measuring Defect Depth in Windows



27 Information Sciences

- 27 Decomposition Algorithm for Global Reachability on a Time-Varying Graph
- 27 Autonomous GN&C for Spacecraft Exploration of Comets and Asteroids
- 28 Efficient Web Services Policy Combination
- 28 Using CTX Image Features to Predict HiRISE-Equivalent Rock Density



31 Bio-Medical

- 31 Isolation of the *Paenibacillus phoenicis*, a Spore-Forming Bacterium
- 31 Monolithically Integrated, Mechanically Resilient Carbon-Based Probes for Scanning Probe Microscopy
- 32 Cell Radiation Experiment System



35 Books & Reports

- 35 Process To Produce Iron Nanoparticle Lunar Dust Simulant Composite
- 35 Inversion Method for Early Detection of ARES-1 Case Breach Failure
- 35 Use of ILTV Control Laws for LaNCETS Flight Research
- 35 Evaluating Descent and Ascent Trajectories Near Non-Spherical Bodies

This document was prepared under the sponsorship of the National Aeronautics and Space Administration. Neither the United States Government nor any person acting on behalf of the United States Government assumes any liability resulting from the use of the information contained in this document, or warrants that such use will be free from privately owned rights.



Portable Handheld Optical Window Inspection Device

This device allows field measurement of defects such as commercial aircraft windows.

John F. Kennedy Space Center, Florida

The Portable Handheld Optical Window Inspection Device (PHOWID) is a measurement system for imaging small defects (scratches, pits, micrometeor impacts, and the like) in the field. Designed primarily for window inspection, PHOWID attaches to a smooth surface with suction cups, and raster scans a small area with an optical pen in order to provide a three-dimensional image of the defect. PHOWID consists of a graphical user interface, motor control subsystem, scanning head, and interface electronics, as well as an integrated camera and user display that allows a user to locate minute defects before scanning. Noise levels are on the order of 60 μm . (1.5 μm).

PHOWID allows field measurement of defects that are usually done in the lab. It is small, light, and attaches directly to the test article in any orientation up to vertical. An operator can scan a defect and get useful engineering data in a matter of minutes. There is no need to make a mold impression for later lab analysis.

The PHOWID system components consist of a scanning head, motor control board, graphical user interface, and supporting electronics, and weighs approximately 5 pounds (2.3 kg). The scanning head consists of an x - y positioner, optical distance sensor, carrier plate, and vacuum supplied suction cups. The head has an integrated camera and LCD (liquid-crystal-display) screen that allows a user to easily position it above the defect. Vacuum is supplied to suction cups through a dual circuit system, which includes check valves to hold the head against the window or other smooth surface up to 90° inclination in the event that the vacuum source is lost. The graphical user interface (GUI) displays the surface image and allows the user to describe an area of interest to be scanned at various speeds and resolutions. The GUI displays the scanning progress in real time. Once a scan is completed, software provides the automated measurement capability to determine defect length, width, and depth and will store this information in a file.

The GUI also communicates with the motion control electronics. These electronics control the x - y positioning motors that move the optical sensor in the sensor head. These electronics also combine the depth and position data in real time and stream the data to the GUI. The associated electronics box contains the vacuum pumps, optical-sensor conditioning electronics, and power supplies.

Functionally, the user places PHOWID over the defect using the integrated camera. The user selects the desired area, resolution, and scan speed at the laptop GUI and initiates scanning. PHOWID has a depth range of 0.01 in. (0.25 mm). It has a noise floor better than 60 μm . (1.5 μm). Usable scan area is on the order of an inch square. Smallest resolution of the scan in the x - y direction is on the order of 300 μm . (7.6 μm).

This work was done by Curtis Ihlefeld and Adam Dokos of Kennedy Space Center and Bradley Burns of ASRC Aerospace Corporation. Further information is contained in a TSP (see page 1). KSC-13218

Salience Assignment for Multiple-Instance Data and Its Application to Crop Yield Prediction

Automated mapping of crops saves on survey time and improves map accuracy.

NASA's Jet Propulsion Laboratory, Pasadena, California

An algorithm was developed to generate crop yield predictions from orbital remote sensing observations, by analyzing thousands of pixels per county and the associated historical crop yield data for those counties. The algorithm determines which pixels contain which crop. Since each known yield value is associated with thousands of individual pixels, this is a "multiple instance" learning problem.

Because individual crop growth is related to the resulting yield, this relationship has been leveraged to identify pixels that are individually related to corn, wheat, cotton, and soybean yield. Those

that have the strongest relationship to a given crop's yield values are most likely to contain fields with that crop. Remote sensing time series data (a new observation every 8 days) was examined for each pixel, which contains information for that pixel's growth curve, peak greenness, and other relevant features.

An alternating-projection (AP) technique was used to first estimate the "salience" of each pixel, with respect to the given target (crop yield), and then those estimates were used to build a regression model that relates input data (remote sensing observations) to the target. This is achieved by constructing

an exemplar for each crop in each county that is a weighted average of all the pixels within the county; the pixels are weighted according to the salience values. The new regression model estimate then informs the next estimate of the salience values. By iterating between these two steps, the algorithm converges to a stable estimate of both the salience of each pixel and the regression model. The salience values indicate which pixels are most relevant to each crop under consideration.

This approach produces better estimates than an existing "primary instance" (PI) approach does. The PI ap-

proach assumes that each county contains a single canonical pixel for each crop (corn, cotton, soybean, etc.) and that the rest of the pixels in that county are noisy observations of the true one.

This work could ultimately provide automated mapping of crops that are

being grown, which could save agencies such as the U.S. Department of Agriculture a significant amount of money that is currently devoted to surveying fields to produce summaries of how much of each crop is being grown. Reliable early estimates of the likely volume

of production can significantly affect crop prices throughout the season.

This work was done by Kiri L. Wagstaff of Caltech and Terran Lane of the University of New Mexico for NASA's Jet Propulsion Laboratory. For more information, contact iaoffice@jpl.nasa.gov. NPO-45177

Speech Acquisition and Automatic Speech Recognition for Integrated Spacesuit Audio Systems

This interface also has applications in mobile phones, in-car devices, and home electronics and appliances.

John H. Glenn Research Center, Cleveland, Ohio

A voice-command human-machine interface system has been developed for spacesuit extravehicular activity (EVA) missions. A multichannel acoustic signal processing method has been created for distant speech acquisition in noisy and reverberant environments. This technology reduces noise by exploiting differences in the statistical nature of signal (i.e., speech) and noise that exists in the spatial and temporal domains. As a result, the automatic speech recognition (ASR) accuracy can be improved to the level at which crewmembers would find the speech interface useful. The developed speech human/machine interface will enable both crewmember usability and operational efficiency. It can enjoy a fast rate of data/text entry, small overall size, and can be lightweight. In addition,

this design will free the hands and eyes of a suited crewmember.

The system components and steps include beam forming/multi-channel noise reduction, single-channel noise reduction, speech feature extraction, feature transformation and normalization, feature compression, model adaptation, ASR HMM (Hidden Markov Model) training, and ASR decoding. A state-of-the-art phoneme recognizer can obtain an accuracy rate of 65 percent when the training and testing data are free of noise. When it is used in spacesuits, the rate drops to about 33 percent. With the developed microphone array speech-processing technologies, the performance is improved and the phoneme recognition accuracy rate rises to 44 percent. The recognizer can be further improved by combining

the microphone array and HMM model adaptation techniques and using speech samples collected from inside spacesuits. In addition, arithmetic complexity models for the major HMM-based ASR components were developed. They can help real-time ASR system designers select proper tasks when in the face of constraints in computational resources.

This work was done by Yiteng (Arden) Huang, Jingdong Chen, and Shaoyan (Sharyl) Chen of WEVOICE, Inc. for Glenn Research Center. Further information is contained in a TSP (see page 1).

Inquiries concerning rights for the commercial use of this invention should be addressed to NASA Glenn Research Center, Innovative Partnerships Office, Attn: Steve Fedor, Mail Stop 4-8, 21000 Brookpark Road, Cleveland, Ohio 44135. Refer to LEW-18534-1.

Predicting Long-Range Traversability From Short-Range Stereo-Derived Geometry

Learning-based software improves obstacle avoidance by robotic ground vehicles.

NASA's Jet Propulsion Laboratory, Pasadena, California

Based only on its appearance in imagery, this program uses close-range 3D terrain analysis to produce training data sufficient to estimate the traversability of terrain beyond 3D sensing range. This approach is called learning from stereo (LFS). In effect, the software transfers knowledge from middle distances, where 3D geometry provides training cues, into the far field where only appearance is available. This is a viable approach because the same obstacle classes, and sometimes the same obstacles, are typi-

cally present in the mid-field and the far-field. Learning thus extends the effective look-ahead distance of the sensors.

The baseline navigation software architecture in both the LAGR (Learning Applied to Ground Robotics) and MTP (Mars Technology Program) programs operates so that stereo image pairs are processed into range imagery, which is then converted to local elevation maps on a ground plane grid with cells roughly 20-cm square covering 5 to 10 m in front of the vehicle, depending on

camera height and resolution. The image and the map are the two basic coordinate systems used, but only pixels with nonzero stereo disparity can be placed into the map. Geometry-based traversability analysis heuristics are used to produce local, grid-based, 'traversability-cost' maps over the local map area, with a real number representing traversability in each map cell. The local elevation and cost maps are accumulated in a global map as the robot drives. Path planning algorithms for local obstacle

avoidance and global route planning are applied to the global map. The resulting path is used to derive steering commands sent to the motor controllers.

The software (training set selection, classifier training, and image classification) runs in real time at about 3 Hz on a 2-GHz processor, and the type of "image appearance features" is user-configurable. Basic RGB (red-green-blue) features, or their powers, or separable textures or within-patch color

histograms can be used in any combination. All of these methods run in real time. The software can work in two modes: purely on-line or by using a fixed, previously-learned classifier. To learn the classifier, a cumulative-training mode is built in which training data across an entire run accumulates, learns a model at the end of the run, and saves the model to a reusable configuration file. The cumulative training mode can run alongside the online classification

mode. One of two classification modes can be used: A linear discriminant (LDA)-based method, or a linear support vector machine (SVM) classifier.

This work was done by Michael Turmon, Benyang Tang, Andrew Howard, and Max Bajracharya of Caltech for NASA's Jet Propulsion Laboratory.

This software is available for commercial licensing. Please contact Daniel Broderick of the California Institute of Technology at danielb@caltech.edu. Refer to NPO-45146.

Browser-Based Application for Telemetry Monitoring of Robotic Assets

NASA's Jet Propulsion Laboratory, Pasadena, California

AEGSE Virtuoso Charting is an application that enables animated, real-time charting of telemetry streams of data from a rover. These automatically scaled charts are completely interactive, and allow users to choose the variables that they want to monitor. The charts can process data from streams with many variables. This application allows for the simultaneous viewing of up to four individually configured charts on a small touch-screen laptop.

The charting application has been tested and found to be extremely robust during long operations. It was left run-

ning overnight, with incoming telemetry at 100 Hz, and it did not experience any signs of lost functionality or memory leaks. This robustness is critical for an application that will be used to support vital tests for the Mars Science Laboratory rover.

The charting component also provides an interactive interface that allows the engineers to decide how many charts they want on their screen, and which attributes should be plotted on each chart. The application is optimized to make the charts on display take up as much of the available space as possible

to maximize the use of the screen real estate. Engineers are also able to plot multiple attributes on the same chart, which enables them to observe the correlation between various attributes.

This work was done by Kelly S. Breed, Mark W. Powell, Khawaja S. Shams, and Richard D. Petras of Caltech for NASA's Jet Propulsion Laboratory. For more information, contact iaoffice@jpl.nasa.gov.

This software is available for commercial licensing. Please contact Daniel Broderick of the California Institute of Technology at danielb@caltech.edu. Refer to NPO-46348.



Miniature Low-Noise G-Band I-Q Receiver

This receiver can be used in humidity sounders for weather forecasting, in broadband communications, and in security imagers.

NASA's Jet Propulsion Laboratory, Pasadena, California

Weather forecasting, hurricane tracking, and atmospheric science applications depend on humidity sounding of atmosphere. Current instruments provide these measurements from ground-based, airborne, and low Earth orbit (LEO) satellites by measuring radiometric temperature on the flanks of the 183-GHz water vapor line. Miniature, low-noise receivers have been designed that will enable these measurements from a geostationary, thinned array sounder, which is based on hundreds of low-noise receivers that convert the 180-GHz signal directly to baseband in-phase and in-quadrature signals for digitization and correlation. The developed receivers provide a noise temperature of 450 K from 165 to 183 GHz (NF = 4.1 dB), and have a mass of 3 g while consuming 24 mW of power. These are the most sensitive broadband I-Q receivers at this frequency range that operate at room temperature, and are significantly lower in mass and power consumption than previously reported receivers.

The receiver development was based on the latest high-performance monolithic millimeter-wave integrated circuit

(MMIC) process. The technology used for the MMICs was 35-nm-gate-length InP HEMT (high electron mobility transistor). It has demonstrated very high transconductance of over 2,000 mS/mm, and sharp turn-on characteristics, which are beneficial for low-noise amplifiers (high transconductance at low drain current). The noise temperature of the receiver is dictated by the first low-noise amplifiers (LNAs) that were slightly modified from the previously reported LNA MMICs. They had three amplifier stages in common source configuration, and passive circuitry was designed with microstrip transmission lines on the 2-mil-thick InP material.

The MMIC LNA has been designed and processed in 35-nm InP technology where the MMIC is $900 \times 600 \mu\text{m}^2$. It is a three-stage design, where each transistor has two gate fingers, for a total of 30 μm gate periphery per device. These LNAs were screened for assembly in the receiver modules by on-wafer measurements.

The LNAs provided the low noise and sufficient gain for the receiver modules, so that an MMIC second harmonic I-Q mixer could be implemented as a resis-

tive balanced mixer. The mixer MMIC was designed in the same 34-nm technology as the LNAs. The quadrature downconversion was implemented with a 90° hybrid coupler (Lange coupler) on the RF side of the mixer. This coupler improved the return loss of the mixer, and achieved broadband 90° phase difference between the two balanced resistive unit mixers. The HEMTs of the mixers had dual gates for balanced LO feed, and they operated biased to below channel pinch-off to maximize the second harmonic content in the channel conduction cycle. The RF signals were directed to the unbiased drains of the mixer HEMTs, and the IF channels were filtered from the drain contacts. A compact and highly efficient power divider and balun were developed for the LO side.

This work was done by Pekka P. Kangaslahti, David M. Pukala, Todd C. Gaier, Alan B. Tanner, Ian J. O'Dwyer, Bjorn H. Lambrigtsen, Mary M. Soria, and Heather R. Owen of Caltech and Richard Lai and Xiaobing Mei of Northrop Grumman Corporation for NASA's Jet Propulsion Laboratory. For more information, contact iaoffice@jpl.nasa.gov. NPO-47442

Methods of Using a Magnetic Field Response Sensor Within Closed, Electrically Conductive Containers

The sensor can be used in containers such as metal fuel tanks.

Langley Research Center, Hampton, Virginia

Magnetic field response sensors are a class of sensors that are powered via oscillating magnetic fields, and when electrically active, respond with their own magnetic fields with attributes dependent upon the magnitude of the physical quantity being measured. A magnetic field response recorder powers and interrogates the magnetic sensors [see "Magnetic-Field-Response Measurement-Acquisition System," *NASA Tech Briefs* Vol. 30, No. 6 (June 2006, page 28)].

Electrically conductive containers have low transmissivity for radio frequency (RF) energy and thus present problems for magnetic field response sensors. It is necessary in some applications to have a magnetic field response sensor's capacitor placed in these containers. Proximity to conductive surfaces alters the inductance and capacitance of the sensors. As the sensor gets closer to a conductive surface, the electric field and magnetic field energy of the sensor is re-

duced due to eddy currents being induced in the conductive surface. Therefore, the capacitors and inductors cannot be affixed to a conductive surface or embedded in a conductive material. It is necessary to have a fixed separation away from the conductive material. The minimum distance for separation is determined by the desired sensor response signal to noise ratio.

Although the inductance is less than what it would be if it were not in prox-

imity to the conductive surface, the inductance is fixed. As long as the inductance is fixed, all variations of the magnetic field response are due to capacitance changes. Numerous variations of inductor mounting can be utilized, such as providing a housing that provides separation from the conductive material as well as protection from impact damage. The sensor can be on the same flexible substrate with a narrow throat portion of the sensor between the inductor and the capacitor, Figure 1. The throat is of sufficient length to allow the capacitor to be appropriately placed within the container and the inductor placed outside the container. The throat is fed through the orifice in the container wall (e.g., fuel tank opening) and connects to the inductor and capacitor via electrical leads, Figure 2. Another embodiment is to have the inductor and capacitor fabricated as separate units. In this embodiment, the inductor is mounted external to the container, and the capacitor is mounted internal to the container, Figure 1. Electrical leads are fed through the orifice to connect the inductor and capacitor, Figure 2.

When a container holding multiple sensors is made of a conductive material, an antenna can be placed internal to the container. An internal antenna allows all components of the sensors to reside inside the container. The antenna must be separated from the container wall's conductive surface. Additionally, the inductors must be maintained in a fixed position relative to and separated from the container wall. Antenna leads are fed through an orifice in the container wall.

This work was done by Stanley E. Woodard of Langley Research Center and Bryant D. Taylor of ATK Space Division. Further information is contained in a TSP (see page 1). LAR-16571-1

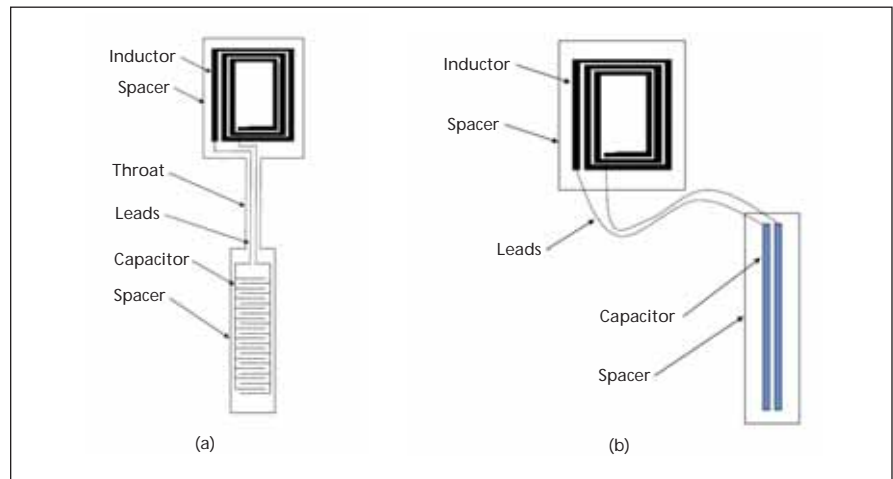


Figure 1. **Magnetic Field Response Sensors** for measurements in conductive containers: (a) Inductor and capacitor on same substrate, (b) Inductor and capacitor on separate substrates.

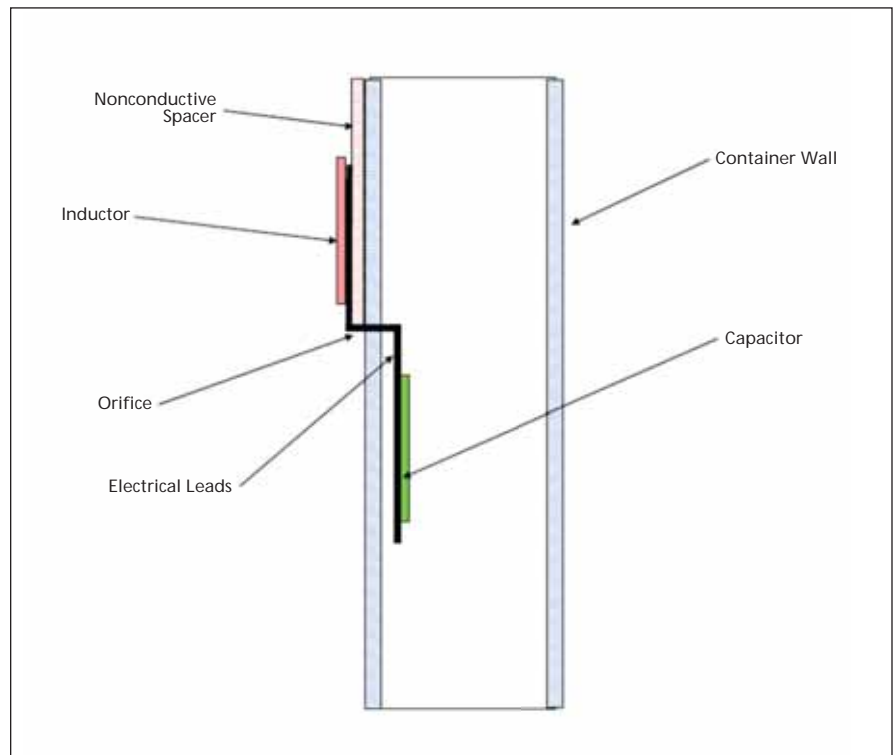


Figure 2. **Cross-Section View:** Magnetic field response sensor for closed electrically conductive container mounted with capacitor within container and inductor external to the container.

Differential Resonant Ring YIG Tuned Oscillator

This oscillator can be used in cognitive radios and for satellite communications.

John H. Glenn Research Center, Cleveland, Ohio

A differential SiGe oscillator circuit uses a resonant ring-oscillator topology in order to electronically tune the oscillator over multi-octave bandwidths. The oscillator's tuning is extremely linear, because the oscillator's frequency depends

on the magnetic tuning of a YIG sphere, whose resonant frequency is equal to a fundamental constant times the DC magnetic field. This extremely simple circuit topology uses two coupling loops connecting a differential pair of SiGe

bipolar transistors into a feedback configuration using a YIG tuned filter creating a closed-loop ring oscillator. SiGe device technology is used for this oscillator in order to keep the transistor's 1/f noise to an absolute minimum in order

to achieve minimum RF phase noise.

The single-end resonant ring oscillator currently has an advantage in fewer parts, but when the oscillation frequency is greater than 16 GHz, the package's parasitic behavior couples energy to the sphere and causes holes and poor phase noise performance. This is because the coupling to the YIG is extremely low, so that the oscillator operates at near the unloaded Q . With the differential resonant ring oscillator, the oscillation currents are just in the YIG coupling mechanisms. The phase noise is even better, and the physical size can be reduced to permit monolithic microwave integrated circuit oscillators.

This invention is a YIG tuned oscillator circuit making use of a differential topology to simultaneously achieve an extremely broadband electronic tuning range and ultra-low phase noise. As a natural result of its differential circuit topology, all reactive elements, such as tuning stubs, which limit tuning bandwidth by contributing excessive open-loop phase shift, have been eliminated. The differential oscillator's open-loop phase shift is associated with completely non-dispersive circuit elements such as the physical angle of the coupling loops, a differential loop crossover, and the high-frequency phase shift of the n-p-n transistors. At the input of the oscillator's feedback loop is a pair of differentially connected n-p-n SiGe transistors that provides extremely high gain, and because they are bulk-effect devices, extremely low $1/f$ noise (leading to ultra-low RF phase noise). The $1/f$ corner frequency for n-p-n SiGe transistors is approximately 500 Hz. The RF energy

from the transistor's collector output is connected directly to the top-coupling loop (the excitation loop) of a single-sphere YIG tuned filter. A uniform magnetic field to bias the YIG must be at a right angle to any vector associated with an RF current in a coupling loop in order for the precession to interact with the RF currents.

In this example, a second bottom coupling loop (the feedback loop) transfers RF energy out of the YIG filter and connects it, in a fully differential configuration, to the input of the differential pair of transistors. The conditions for start oscillation for a ring oscillator require that its open-loop phase shift be equal to $N(360^\circ)$, where N is an integer equal to 0, 1, 2, 3 ... , and its open-loop gain must be greater than 1.0 (or 0 dBs). The electrical phase shift associated with the relative coupling loop to coupling loop physical angle is simply equal to the relative angle between the loops, which is usually -90° . The choice of 90° is important because it places the RF magnetic fields of the two loops in quadrature, which prevents any RF energy coupling between the two loops unless it is coupled through the mechanism of the YIG sphere's resonance, which is a chief source of spurious oscillations. The direction of the magnetic field is important because the sign of the phase shift depends on the direction of the magnetic field.

In one magnetic bias field direction, the oscillator will oscillate, and in the other direction, the oscillator will not oscillate over the designed frequency range. The differential output from the

transistor pair is a perfect configuration match for the naturally differential coupling loops of this YIG tuned filter. The YIG filter has a Q of greater than 1,000, significantly contributing to the excellent overall phase noise of the oscillator. Therefore, the differential oscillator's electronic tuning can achieve multiple octaves of tuning, perhaps approaching a full decade. Oscillations will naturally occur at all frequencies for which the YIG sphere is tuned, magnetically biased to resonance by the DC magnetic bias field, without the need to make adjustments of any kind to a frequency selective reactive network, such as a tuning stub. By eliminating the need for making alignment adjustments, the differential oscillator is expected to have low-cost manufacturing. Output from this oscillator can be taken from the collectors in a differential manner, assuring that a balance is maintained to keep both transistor collectors at the same impedance, or from a third separate coupling loop which has the advantage of being a tracking filter on the output RF.

Since SiGe technology has a f_t in excess of 100 GHz, this oscillator circuit can be made to operate at frequencies in excess of 50 GHz.

This work was done by Ronald A. Parrott of VIDA Products, Inc. for Glenn Research Center. Further information is contained in a TSP (see page 1).

Inquiries concerning rights for the commercial use of this invention should be addressed to NASA Glenn Research Center, Innovative Partnerships Office, Attn: Steven Fedor, Mail Stop 4-8, 21000 Brookpark Road, Cleveland, Ohio 44135. Refer to LEW-18512-1.



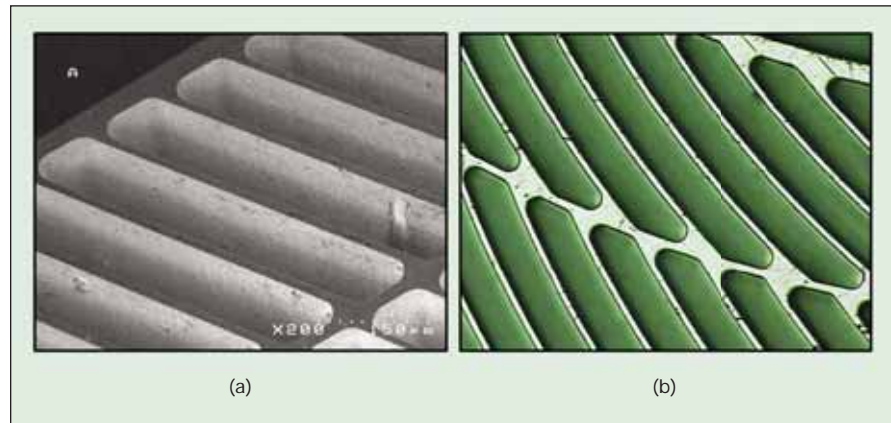
Microfabricated Segmented-Involute-Foil Regenerator for Stirling Engines

Tests show significantly improved performance.

John H. Glenn Research Center, Cleveland, Ohio

An involute-foil regenerator was designed, microfabricated, and tested in an oscillating-flow test rig. The concept consists of stacked involute-foil nickel disks (see figure) microfabricated via a lithographic process. Test results yielded a performance of about twice that of the 90-percent random-fiber currently used in small Stirling converters.

The segmented nature of the involute-foil in both the axial and radial directions increases the strength of the structure relative to wrapped foils. In addition, relative to random-fiber regenerators, the involute-foil has a reduced pressure drop, and is expected to be less susceptible to the release of metal fragments into the working space, thus increasing reliability. The prototype nickel involute-foil regenerator was adequate for testing in an engine with a 650 °C hot-end temperature. This is lower than that required by larger engines, and high-temperature alloys are not suited for the lithographic microfabrication approach.



Micrographs of Regenerator Disks are shown during the final steps of fabrication: (a) micrograph of features with remaining PMMA removed and (b) picture of nickel ribs after removal from substrate.

This work was done by Mounir Ibrahim and Daniel Danila of Cleveland State University; Terrence Simon, Susan Mantell, and Liyong Sun of the University of Minnesota; David Gedeon of Gedeon Associates; Song-gang Qiu of Infinia Corp.; Gary Wood of Sunpower Inc.; and Kevin Kelly and Jeffrey McLean of International Mezzo Technologies

for Glenn Research Center. Further information is contained in a TSP (see page 1).

Inquiries concerning rights for the commercial use of this invention should be addressed to NASA Glenn Research Center, Innovative Partnerships Office, Attn: Steve Fedor, Mail Stop 4-8, 21000 Brookpark Road, Cleveland, Ohio 44135. Refer to LEW-18431-1.

Reducing Seal Adhesion in Low Impact Docking Systems

Atomic oxygen is used to treat mating silica surfaces to reduce unwanted adhesion during docking/undocking operations.

John H. Glenn Research Center, Cleveland, Ohio

Silicone elastomers, used in seals for airlocks or other sealing surfaces in space, are sticky in their as-received condition. Because of the sticking, a greater force may be needed to separate the mating surfaces. If the adhesion is sufficiently high, a sudden unpredictable movement of the spacecraft during undocking, vibration, or uneven release could pull off the seal, resulting in a damage that would have to be repaired before another docking. The damaged seal can result in significant gas leakage and possibly in a cata-

strophic mishap impacting the safety of the crew. It is also possible that a compromised seal could result in a delayed but sudden gas leak that could put the crew at unexpected risk. This is especially of concern for androgynous seals, which have identical mating surfaces on both sides for interchangeability and redundancy. Such seals typically have elastomer-on-elastomer sealing surfaces. To reduce sticking, one could use release agents such as powders and lubricants, but these can be easily removed and transferred to other sur-

faces, causing uneven sealing and contamination. Modification of the elastomer surface to make a more slippery and less sticky surface that is integral with the bulk elastomer would be more desirable.

The analysis of materials retrieved from early space shuttle missions such as the Long Duration Exposure Facility indicated that silicone surfaces were converted to SiO₂ silica glass as a result of the low Earth orbital atomic oxygen exposure. With a controlled atomic oxygen exposure, the converted silica

surface is integral with the underlying silicone and is sufficiently thin enough that the elastomers retain their flexibility and sealing properties, yet the silicone does not stick to surfaces because the surface is essentially a thin film of SiO₂ glass.

Silicone seals are mounted on the surface of electrically grounded aluminum exposure plates or suspended such that the interfacing silicone seal surfaces are exposed to a low-pressure atmospheric plasma. The seal surfaces are then exposed to atomic oxygen, until the desired reduction in seal adhesion is achieved. Polyimide Kapton H

atomic oxygen fluence witness samples are also placed into the vacuum chamber during air plasma exposure to measure the Kapton effective fluence by weight loss of vacuum dehydrated Kapton H samples.

Functional operation of the seals is such that the atomic oxygen treated surface will then interface during docking with another atomic oxygen treated surface or a metal surface. Thus, the mating is between two opposing silica surfaces on silicone or silica surfaces on smooth metal surfaces.

The atomic oxygen treated silicone seal geometry can be varied as well as

the composition of the silicone. Parts of the seal can be treated rather than all of the seal if it is desirable to have adhesion in a specific direction or at a specific interface.

This work was done by Bruce A. Banks and Sharon K. Miller of Glenn Research Center. Further information is contained in a TSP (see page 1).

Inquiries concerning rights for the commercial use of this invention should be addressed to NASA Glenn Research Center, Innovative Partnerships Office, Attn: Steven Fedor, Mail Stop 4-8, 21000 Brookpark Road, Cleveland, Ohio 44135. Refer to LEW-18572-1.

Optimal Flow Control Design

This design results in a quieter and more environmentally friendly transport aircraft.

Langley Research Center, Hampton, Virginia

In support of the Blended-Wing-Body aircraft concept, a new flow control hybrid vane/jet design has been developed for use in a boundary-layer-ingesting (BLI) offset inlet in transonic flows. This inlet flow control is designed to minimize the engine fan-face distortion levels and the first five Fourier harmonic half amplitudes while maximizing the inlet pressure recovery. This concept represents a potentially enabling technology for quieter and more environmentally friendly transport aircraft.

An optimum vane design was found by minimizing the engine fan-face distortion, DC60, and the first five Fourier harmonic half amplitudes, while maximizing the total pressure recovery. The optimal vane design was then used in a BLI inlet wind tunnel experiment at NASA Langley's 0.3-meter transonic cryogenic tunnel. The experimental re-

sults demonstrated an 80-percent decrease in DPCPavg, the reduction in the circumferential distortion levels, at an inlet mass flow rate corresponding to the middle of the operational range at the cruise condition.

Even though the vanes were designed at a single inlet mass flow rate, they performed very well over the entire inlet mass flow range tested in the wind tunnel experiment with the addition of a small amount of jet flow control. While the circumferential distortion was decreased, the radial distortion on the outer rings at the aerodynamic interface plane (AIP) increased. This was a result of the large boundary layer being distributed from the bottom of the AIP in the baseline case to the outer edges of the AIP when using the vortex generator (VG) vane flow control.

Experimental results, as already mentioned, showed an 80-percent reduction of DPCPavg, the circumferential distortion level at the engine fan-face. The hybrid approach leverages strengths of vane and jet flow control devices, increasing inlet performance over a broader operational range with significant reduction in mass flow requirements. Minimal distortion level requirements are met using vanes alone, avoiding engine stall and increasing robustness of this hybrid inlet flow control approach. This design applies to aerospace applications needing flush-mounted boundary-layer-ingesting inlets.

This work was done by Brian Allan and Lewis Owens of Langley Research Center. For further information, contact the Langley Innovative Partnerships Office at (757) 864-8881. LAR-17365-1

Corrosion-Resistant Container for Molten-Material Processing

A combination of materials functions and survives in hot, corrosive environments.

John H. Glenn Research Center, Cleveland, Ohio

In a carbothermal process, gaseous methane is passed over molten regolith, which is heated past its melting point to a temperature in excess of 1,625 °C. At this temperature, materials in contact with the molten regolith (or regolith simulant) corrode and lose their structural properties. As a result, fabricating a crucible to hold the molten material and

providing a method of contact heating have been problematic.

Alternative containment approaches use a large crucible and limit the heat zone of the material being processed, which is inefficient because of volume and mass constraints. Alternative heating approaches use non-contact heating, such as by laser or concentrated solar en-

ergy, which can be inefficient in transferring heat and thus require higher power heat sources to accomplish processing.

The innovation is a combination of materials, with a substrate material having high structural strength and stiffness and high-temperature capability, and a coating material with a high corrosion resistance and high-temperature capa-

bility. The material developed is a molybdenum substrate with an iridium coating. Creating the containment crucible or heater jacket using this material combination requires only that the molybdenum, which is easily processed by conventional methods such as milling, electric discharge machining, or forming and brazing, be fabricated into an appropriate shape, and that the iridium coating be applied to any surfaces that may come in contact with the corrosive molten material.

In one engineering application, the molybdenum was fashioned into a con-

tainer for a heat pipe. Since only the end of the heat pipe is used to heat the regolith, the container has a narrowing end with a nipple in which the heat pipe is snugly fit, and the external area of this nipple, which contacts the regolith to transfer heat into it, is coated with iridium.

At the time of this reporting, no single material has been found that can perform the functions of this combination of materials, and other combinations of materials have not proven to be survivable to the corrosiveness of this environment.

High-temperature processing of materials with similar constituencies as lunar regolith is fairly common. The carbothermal process is commonly used to make metallurgical-grade silicon for the semiconductor and solar-cell industries.

This work was done by Theodore G. Stern and Eric McNaul of DR Technologies for Glenn Research Center.

Inquiries concerning rights for the commercial use of this invention should be addressed to NASA Glenn Research Center, Innovative Partnerships Office, Attn: Steve Fedor, Mail Stop 4-8, 21000 Brookpark Road, Cleveland, Ohio 44135. Refer to LEW-18459-1.



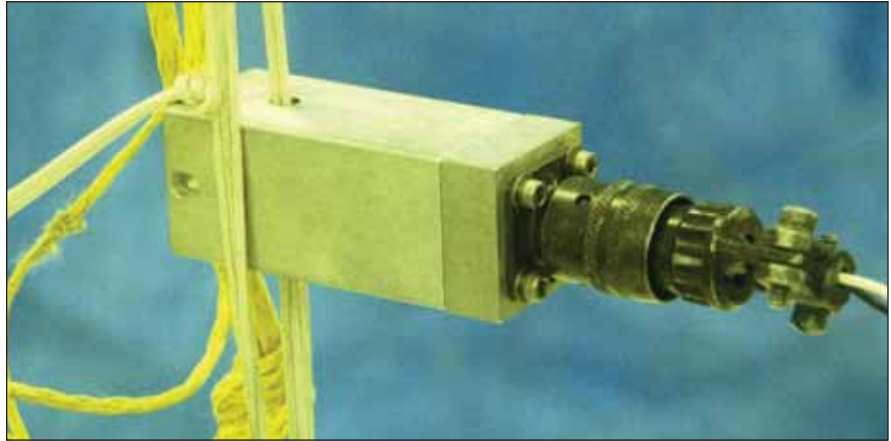
Reusable Hot-Wire Cable Cutter

This device can be used to cut any type of small synthetic cable.

NASA's Jet Propulsion Laboratory, Pasadena, California

During the early development stage of balloon deployment systems for missions, nichrome wire cable cutters were often used in place of pyro-actuated cutters. Typically, a nichrome wire is wrapped around a bundle of polymer cables with a low melting point and connected to a relay-actuated electric circuit. The heat from the nichrome reduces the strength of the cable bundle, which quickly breaks under a mechanical load and can thus be used as a release mechanism for a deployment system. However, the use of hand-made heated nichrome wire for cutters is not very reliable. Often, the wrapped nichrome wire does not cut through the cable because it either pulls away from its power source or does not stay in contact with the cable being cut. Because nichrome is not readily soldered to copper wire, unreliable mechanical crimps are often made to connect the nichrome to an electric circuit.

A self-contained device that is reusable and reliable was developed to sever cables for device release or deployment. The nichrome wire in this new device is housed within an enclosure to prevent it from being damaged by handling. The electric power leads are internally connected within the unit to the nichrome wire using a screw terminal connection. A bayonet plug, a quick and secure method of connecting the cutter to the power source, is used to connect the cutter to the power leads similar to those used in pyro-cutter devices.



The Reusable Hot-Wire Cable Cutter installed on a deployment line.

A small ceramic tube [0.25-in. wide 0.5-in. long (\approx 6.4-mm wide 13-mm long)] houses a spiraled nichrome wire that is heated when a cable release action is required. The wire is formed into a spiral coil by wrapping it around a mandrel. It is then laid inside the ceramic tube so that it fits closely to the inner surface of the tube. The ceramic tube provides some thermal and electrical insulation so that most of the heat generated by the wire is directed toward the cable bundle in the center of the spiral. The ceramic tube is cemented into an aluminum block, which holds it in position. The leads of the nichrome wire are attached to screw terminals that connect them to power leads. A bayonet plug mounted at the bottom of the rectangular block connects the power leads to a relay circuit. A

thin aluminum shell encloses the entire structure, leaving access points to attach to the bayonet plug and to feed a cable into the cylinder. The access holes for the deployment cable are a smaller diameter than the nichrome coil to prevent the cable from coming in direct contact with the nichrome when loaded.

It uses the same general method of severing a cable with a heated wire as was used previously, but implements it in such a way that it is more reliable and less prone to failure. It creates a mechanism to create repeatability that was nonexistent in the previous method.

This work was done by Michael T. Pauken and Joel M. Steinkraus of Caltech for NASA's Jet Propulsion Laboratory. Further information is contained in a TSP (see page 1). NPO-47265

Deployment of a Curved Truss

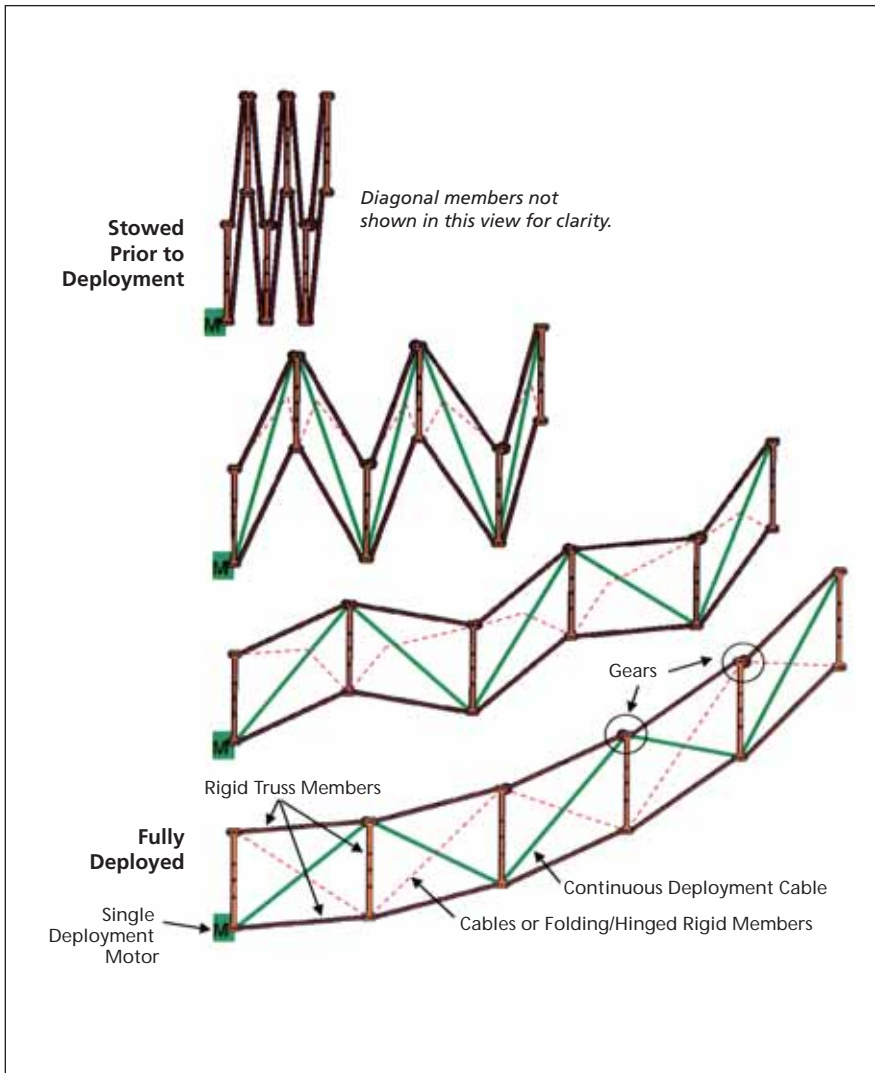
This structure is potentially useful to the military or emergency service providers to rapidly deploy enclosures for shelter or storage.

NASA's Jet Propulsion Laboratory, Pasadena, California

Structures capable of deployment into complex, three-dimensional trusses have well known space technology applications such as the support of spacecraft payloads, communications antennas, radar

reflectors, and solar concentrators. Such deployable trusses could also be useful in terrestrial applications such as the rapid establishment of structures in military and emergency service situations, in particular

with regard to the deployment of enclosures for habitat or storage. To minimize the time required to deploy such an enclosure, a single arch-shaped truss is preferable to multiple straight trusses



The Deployment Sequence of the Truss. The truss is stowed in a compact volume (top), and deployment begins when the motor is activated and begins drawing in the continuous deployment cable (bottom).

arranged vertically and horizontally. To further minimize the time required to deploy such an enclosure, a synchronous deployment with a single degree of freedom is also preferable.

One method of synchronizing deployment of a truss is the use of a series of gears; this makes the deployment sequence predictable and testable, allows the truss to have a minimal stowage volume, and the deployed structure exhibits the excellent stiffness-to-mass and strength-to-mass ratios characteristic of a truss. A concept for using gears with varying ratios to deploy a truss into a curved shape has been developed and appears to be compatible with both space technology applications as well as potential use in terrestrial applications such as enclosure deployment. As is the case with other deployable trusses, this truss is formed using rigid truss elements (e.g., composite tubes) along the edges, one set of diagonal elements composed of either cables or folding/hinged rigid members, and the other set of diagonal elements formed by a continuous cable that is tightened by a motor or hand crank in order to deploy the truss. Gears of varying ratios are used to constrain the deployment to a single degree of freedom, making the deployment synchronous, predictable, and repeatable. The relative sizes of the gears and the relative dimensions of the diagonal elements determine the deployed geometry (e.g. curvature) of the truss.

This work was done by Louis R. Giersch and Kevin Knarr of Caltech for NASA's Jet Propulsion Laboratory. Further information is contained in a TSP (see page 1). NPO-47269

⚙️ High-Volume Airborne Fluids Handling Technologies To Fight Wildfires

Airborne flame retardants are used in a highly efficient firefighting system.

Dryden Flight Research Center, Edwards, California

NASA recently partnered with the U.S. Forest Service (USFS) on a project to examine mission suitability and recommend policies and procedures for the use of very large aerial firefighting aircraft such as the Boeing 747 and DC-10 aerial retardant delivery aircraft. The aircraft under study included a 10Tanker DC-10 and an Evergreen B-747. NASA's Dryden Flight Research Center and Ames Research Center worked with the USFS to help deter-

mine the safe flight envelope for these Very Large Air Tanker (VLAT) aircraft for the USFS and the Department of the Interior (DOI). This new generation of "supertankers" includes aircraft like these that have as much as four times the delivery capacity of the previous generation of aerial firefighting aircraft.

Dryden performed operational test and evaluation assessments and reported findings and recommendations on these aircraft in cooperation with

Ames. The team developed, implemented, and directed an evaluation test plan for use in flight test and in simulation. Ames provided support using pilot-in-the-loop simulations and coordinated simulator models, flight profiles, and data analysis with Dryden. The test plan was designed to evaluate the suitability of VLAT aircraft as a function of mission environment. Based on this analysis, NASA generated interim flight envelope limitations to enhance safety and opera-

tional utility in the fire-retardant delivery mission. These recommended flight limitations were adopted by the USFS.

The 10Tanker DC-10 has been in use for several years with the California Department of Forestry and Fire Protection (Cal-Fire), but until NASA took on the challenge of reviewing VLAT capabilities and limitations, the USFS was hesitant to add them to the federal wildfire arsenal. The DC-10 delivery system is based on an externally mounted set of tanks and a "bomb-bay style" set of clamshell doors that are opened in precisely calibrated ways to deliver the amounts and concentrations of retardant called for by the specific wildfire situation. The system was manufactured by Jordan Air of Central Point, OR, and was installed by Victorville Aerospace in

Victorville, CA. It can deliver 12,000 gallons (45.4 kL) of retardant in as little as eight seconds. The aircraft can deliver a partial load of retardant and make multiple drops on the same flight, or the entire load can be rapidly delivered in one pass if required for maximum coverage.

The Evergreen 747 uses internal tankage and a pressurized delivery system to enable volume and coverage levels that also meet USFS requirements, but enables computer control of flow for desired precision. This system was designed and built by Adaptive Aerospace of Tehachapi, CA and can deliver about 20,000 gallons (75.7 kL) of retardant in approximately ten seconds. The 747 can also make multiple independent drops, or deliver the entire load at once.

NASA found that both of these VLAT aircraft are compatible with the wildfire suppression mission when used to supplement other aerial retardant delivery platforms. The major recommendations for deployment that resulted from this study relate to terrain clearance, the type of terrain in the drop area, availability of qualified lead planes to guide the VLAT approach to the drop area, and low-altitude maneuvering limitations. NASA's analysis suggests that with the appropriate flight procedures, these aircraft will provide a powerful set of tools to fight wildfires.

This work was done by Mark Dickerson and Timothy Cox of Dryden Flight Research Center, Cliff Hale of Evergreen International Aviation, Inc., and Rick Hatton of 10Tanker Air Carrier. Further information is contained in a TSP (see page 1). DRC-010-019



Modeling of Alkane Oxidation Using Constituents and Species

This methodology is of interest to automobile manufacturers and other gas-turbine engine manufacturers.

NASA's Jet Propulsion Laboratory, Pasadena, California

It is currently not possible to perform simulations of turbulent reactive flows due in particular to complex chemistry, which may contain thousands of reactions and hundreds of species. This complex chemistry results in additional differential equations, making the numerical solution of the equation set computationally prohibitive. Reducing the chemical kinetics mathematical description is one of several important goals in turbulent reactive flow modeling. A chemical kinetics reduction model is proposed for alkane oxidation in air that is based on a parallel methodology to that used in turbulence modeling in the context of the Large Eddy Simulation. The objective of kinetic modeling is to predict the heat release and temperature evolution. This kinetic mechanism is valid over a pressure range from atmospheric to 60 bar, temperatures from 600 K to 2,500 K, and equivalence ratios from 0.125 to 8. This range encompasses diesel, HCCI, and gas-turbine engines, including cold ignition.

A computationally efficient kinetic reduction has been proposed for alkanes that has been illustrated for n-heptane using the LLNL heptane mechanism. This model is consistent with turbulence modeling in that scales were first categorized into either those modeled or those computed as progress variables. Species were identified as being either light or heavy. The heavy species were decomposed into defined 13 constituents, and their total molar density was shown to evolve in a quasi-steady manner. The light species behave either in a quasi-steady or unsteady manner. The modeled scales are the total constituent molar density, N_c , and the molar density of the quasi-steady light species.

The progress variables are the total constituent molar density rate evolution and the molar densities of the unsteady light species. The unsteady equations for the light species contain contributions of the type gain/loss rates from the heavy species that are modeled consistent with the developed mathematical forms for the total constituent molar

density rate evolution; indeed, examination of these gain/loss rates shows that they also have a good quasi-steady behavior with a functional form resembling that of the constituent rate. This finding highlights the fact that the fitting technique provides a methodology that can be repeatedly used to obtain an accurate representation of full or skeletal kinetic models.

Assuming success with the modified reduced model, the advantage of the modeling approach is clear. Because this model is based on the N_c rate rather than on that of individual heavy species, even if the number of species increases with increased carbon number in the alkane group, providing that the quasi-steady rate aspect persists, then extension of this model to higher alkanes should be conceptually straightforward, although it remains to be seen if the functional fits would remain valid or would require reconstruction.

This work was done by Josette Bellan and Kenneth G. Harstad of Caltech for NASA's Jet Propulsion Laboratory. For more information, contact iaoffice@jpl.nasa.gov. NPO-46792

Fabrication of Lanthanum Telluride 14-1-11 Zintl High-Temperature Thermoelectric Couple

This methodology will aid device fabrication for waste energy recovery applications in cars, power plants, and industrial processes and machinery.

NASA's Jet Propulsion Laboratory, Pasadena, California

The development of more efficient thermoelectric couple technology capable of operating with high-grade heat sources up to 1,275 K is key to improving the performance of radioisotope thermoelectric generators. Lanthanum telluride $\text{La}_{3-x}\text{Te}_4$ and 14-1-11 Zintl ($\text{Yb}_{14}\text{MnSb}_{11}$) have been identified as very promising materials.

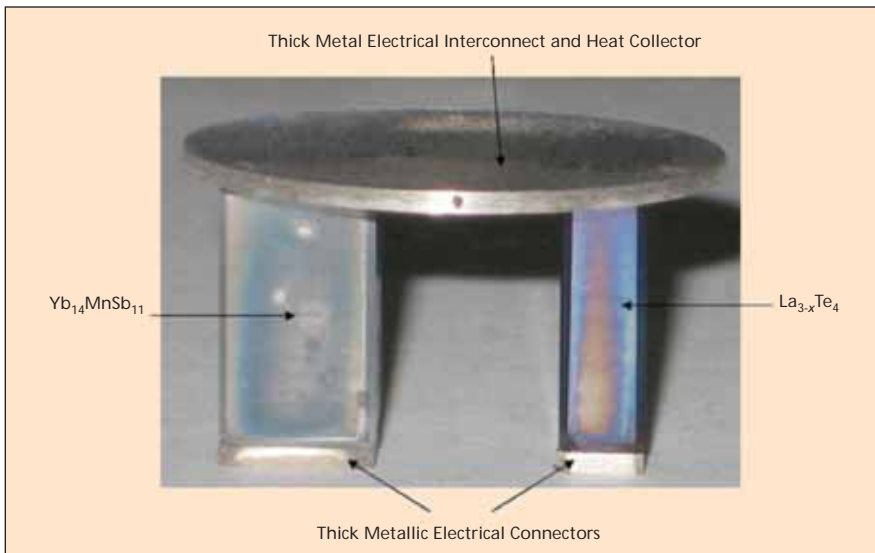
The fabrication of advanced high-temperature thermoelectric couples requires the joining of several dissimilar materials, typically including a number of diffusion

bonding and brazing steps, to achieve a device capable of operating at elevated temperatures across a large temperature differential (up to 900 K). A thermoelectric couple typically comprises a heat collector/exchanger, metallic interconnects on both hot and cold sides, n-type and p-type conductivity thermoelectric elements, and cold-side hardware to connect to the cold-side heat rejection and provide electrical connections.

Differences in the physical, mechanical, and chemical properties of the materials

that make up the thermoelectric couple, especially differences in the coefficients of thermal expansion (CTE), result in undesirable interfacial stresses that can lead to mechanical failure of the device. The problem is further complicated by the fact that the thermoelectric materials under consideration have large CTE values, are brittle, and cracks can propagate through them with minimal resistance.

The inherent challenge of bonding brittle, high-thermal-expansion thermoelectric materials to a hot shoe material



The High-Temperature Couple made of $\text{La}_{3-x}\text{Te}_4$ and $\text{Yb}_{14}\text{MnSb}_{11}$.

that is thick enough to carry the requisite electrical current was overcome. A critical advantage over prior art is that this device was constructed using all diffusion bonds and a minimum number of assembly steps.

The fabrication process and the materials used are described in the following steps:

(1) Applying a thin refractory metal foil to both sides of lanthanum tel-

luride. To fabricate the n-type leg of the advanced thermoelectric couple, the pre-synthesized lanthanum telluride coupon was diffusion bonded to the metal foil using a thin adhesion layer.

(2) Repeating a similar process for the 14-1-11 Zintl p-type leg of the advanced thermoelectric couple.

(3) Bonding thick CTE-matched metal plates on the metallized lanthanum

telluride and $\text{Yb}_{14}\text{MnSb}_{11}$ to form the hot and cold sides of the thermoelectric couple.

The calculated conversion efficiency of such an advanced couple would be about 10.5 percent, about 35 percent better than heritage radioisotope thermoelectric technology that relies on Si-Ge alloys. In addition, unlike Si-Ge alloys, these materials can be combined with many other thermoelectric materials optimized for operation at lower temperatures to achieve conversion efficiency in excess of 15 percent (a factor of 2 increase over heritage technology).

This work was done by Vilupanur A. Ravi, Billy Chun-Yip Li, and Jean-Pierre Fleurial of Caltech and Kurt Star of UCLA for NASA's Jet Propulsion Laboratory. Further information is contained in a TSP (see page 1).

In accordance with Public Law 96-517, the contractor has elected to retain title to this invention. Inquiries concerning rights for its commercial use should be addressed to:

*Innovative Technology Assets Management
JPL*

Mail Stop 202-233

4800 Oak Grove Drive

Pasadena, CA 91109-8099

E-mail: iaoffice@jpl.nasa.gov

Refer to NPO-46655, volume and number of this NASA Tech Briefs issue, and the page number.

A Computer Model for Analyzing Volatile Removal Assembly

John H. Glenn Research Center, Cleveland, Ohio

A computer model simulates reactional gas/liquid two-phase flow processes in porous media. A typical process is the oxygen/wastewater flow in the Volatile Removal Assembly (VRA) in the Closed Environment Life Support System (CELSS) installed in the International Space Station (ISS). The volatile organics in the wastewater are combusted by oxygen gas to form clean water and carbon dioxide, which is solved in the water phase. The model

predicts the oxygen gas concentration profile in the reactor, which is an indicator of reactor performance.

In this innovation, a mathematical model is included in the computer model for calculating the mass transfer from the gas phase to the liquid phase. The amount of mass transfer depends on several factors, including gas-phase concentration, distribution, and reaction rate. For a given reactor dimension, these factors depend on pressure and

temperature in the reactor and composition and flow rate of the influent.

This work was done by Boyun Guo of the University of Louisiana at Lafayette for Glenn Research Center. Further information is contained in a TSP (see page 1).

Inquiries concerning rights for the commercial use of this invention should be addressed to NASA Glenn Research Center, Innovative Partnerships Office, Attn: Steve Fedor, Mail Stop 4-8, 21000 Brookpark Road, Cleveland, Ohio 44135. Refer to LEW-18369-1.



Analysis of Nozzle Jet Plume Effects on Sonic Boom Signature

Highly underexpanded nozzle flow provides reduction in tail shock strength.

Dryden Flight Research Center, Edwards, California

An axisymmetric full Navier-Stokes computational fluid dynamics (CFD) study was conducted to examine nozzle exhaust jet plume effects on the sonic boom signature of a supersonic aircraft. A simplified axisymmetric nozzle geometry, representative of the nozzle on the NASA Dryden NF-15B Lift and Nozzle Change Effects on Tail Shock (LaNCETS) research airplane, was considered. The highly underexpanded nozzle flow is found to provide significantly more reduction in the tail shock strength in the sonic boom N-wave pressure signature than perfectly expanded and overexpanded nozzle flows. A tail shock train in the sonic boom signature, similar to what was observed in the LaNCETS flight data, is observed for the highly underexpanded nozzle flow. The CFD results provide a detailed description of the nozzle flow physics involved in the LaNCETS nozzle at different nozzle expansion conditions and help in interpreting LaNCETS flight data as well as in the eventual CFD analysis of a full LaNCETS aircraft. The current study also provided important information on proper modeling of the LaNCETS aircraft nozzle.

The primary objective of the current CFD research effort was to support the LaNCETS flight research data analysis effort by studying the detailed nozzle exhaust jet plume's imperfect expansion effects on the sonic boom signature of a supersonic aircraft. Figure 1 illustrates the primary flow physics present in the interaction between the exhaust jet plume shock and the sonic boom coming off of an axisymmetric body in supersonic flight. The steeper tail shock from highly expanded jet plume reduces the dip of the sonic boom N-wave signature. A structured finite-volume compressible full Navier-Stokes CFD code was used in the current study. This approach is not limited by the simplifying assumptions inherent in previous sonic boom analysis efforts. Also, this study was the first known jet plume sonic boom CFD study in which the full viscous nozzle flow field was modeled, without coupling to a

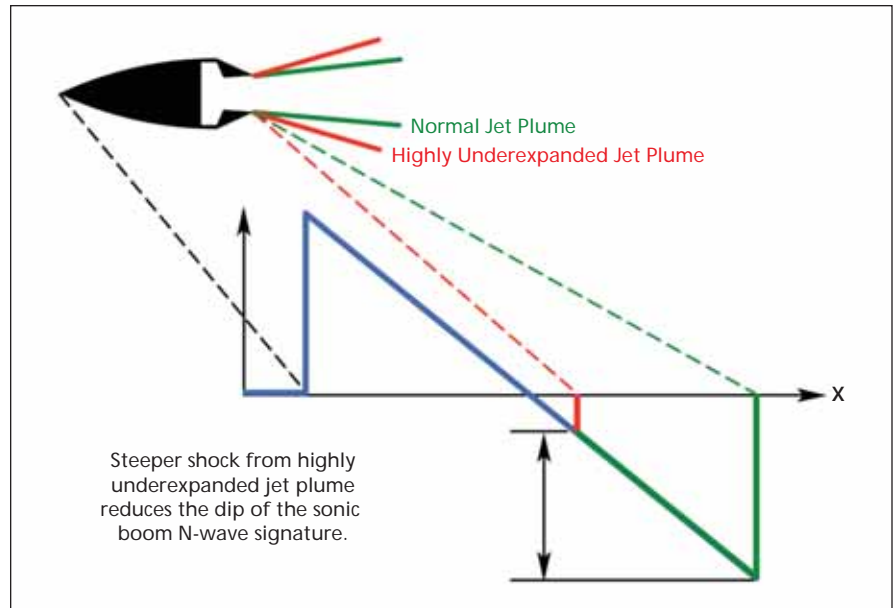


Figure 1. Jet Plume Shock—sonic boom interaction flow physics.

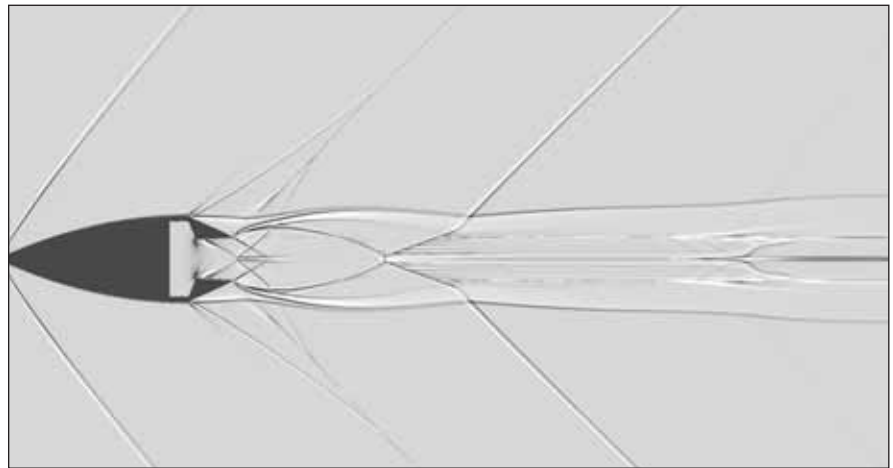


Figure 2. A CFD Shadowgraph visualization of imperfectly expanded jet plume effects.

sonic boom propagation analysis code, from the stagnation chamber of the nozzle to the far field external flow, taking into account all nonisentropic effects in the shocks, boundary layers, and free shear layers, and their interactions at distances up to 30 times the nozzle exit diameter from the jet centerline. A CFD solution is shown in Figure 2. The flow field is very complicated and multi-

dimensional, with shock-shock and shock-plume interactions. At the time of this reporting, a full three-dimensional CFD study was being conducted to evaluate the effects of nozzle vectoring on the aircraft tail shock strength.

This work was done by Trong Bui of Dryden Flight Research Center. Further information is contained in a TSP (see page 1). DRC-009-032

Optical Sidebands Multiplier

NASA's Jet Propulsion Laboratory, Pasadena, California

Optical sidebands have been generated with relative frequency tens to hundreds of GHz by using optical sidebands that are generated in a cascade process in high-quality optical resonators with Kerr nonlinearity, such as whispering gallery mode (WGM) resonators. For this purpose, the WGM resonator needs to be optically pumped at two frequencies matching its resonances. These two optical components can be one or several free spectral ranges (FSRs), equal to approximately 12 GHz, in this example, apart from each other, and can be easily derived from a monochromatic pump with an ordinary EOM (electro-optic

modulation) operating at half the FSR frequency. With sufficient nonlinearity, an optical cascade process will convert the two pump frequencies into a comb-like structure extending many FSRs around the carrier frequency. This has a demonstratively efficient frequency conversion of this type with only a few milliwatt optical pump power.

The concept of using Kerr nonlinearity in a resonator for non-degenerate wave mixing has been discussed before, but it was a common belief that this was a weak process requiring very high peak powers to be observable. It was not thought possible for this ap-

proach to compete with electro-optical modulators in CW applications, especially those at lower optical powers. By using the high-Q WGM resonators, the effective Kerr nonlinearity can be made so high that, using even weak seeding bands available from a conventional EOM, one can effectively multiply the optical sidebands, extending them into an otherwise inaccessible frequency range.

This work was done by Dmitry V. Strelakov and Nan Yu of Caltech for NASA's Jet Propulsion Laboratory. Further information is contained in a TSP (see page 1). NPO-47322

Single Spatial-Mode Room-Temperature-Operated 3.0 to 3.4 μm Diode Lasers

These devices can be used in gas sensing for environmental monitoring.

NASA's Jet Propulsion Laboratory, Pasadena, California

Compact, highly efficient, 3.0 to 3.4 μm light emitters are in demand for spectroscopic analysis and identification of chemical substances (including methane and formaldehyde), infrared countermeasures technologies, and development of advanced infrared scene projectors. The need for these light emitters can be currently addressed either by bulky solid-state light emitters with limited power conversion efficiency, or cooled Interband Cascade (IC) semiconductor lasers.

Researchers here have developed a breakthrough approach to fabrication of diode mid-IR lasers that have several advantages over IC lasers used for the Mars 2009 mission. This breakthrough is due to a novel design utilizing the strain-engi-

neered quantum-well (QW) active region and quaternary barriers, and due to optimization of device material composition and growth conditions (growth temperatures and rates). However, in their present form, these GaSb-based laser diodes cannot be directly used as a part of sensor systems. The device spectrum is too broad to perform spectroscopic analysis of gas species, and operating currents and voltages are too high.

In the current work, the emitters were fabricated as narrow-ridge waveguide index-guided lasers rather than broad stripe-gain guided multimode Fabry-Perot (FP) lasers as was done previously. These narrow-ridge waveguide mid-IR lasers exhibit much lower power consumptions, and can operate in a single

spatial mode that is necessary for demonstration of single-mode distributed feedback (DBF) devices for spectroscopic applications.

These lasers will enable a new generation of compact, tunable diode laser spectrometers with lower power consumption, reduced complexity, and significantly reduced development costs. These lasers can be used for the detection of HCN, C_2H_2 , methane, and ethane.

This work was done by Siamak Forouhar, Clifford F. Frez, and Alexander Soibel of Caltech and Gregory Belenky, Leon Shterengas, and Gela Kipshidze of The State University of New York at Stony Brook for NASA's Jet Propulsion Laboratory. For more information, contact iaoffice@jpl.nasa.gov. NPO-47377

Self-Nulling Beam Combiner Using No External Phase Inverter

NASA's Jet Propulsion Laboratory, Pasadena, California

A self-nulling beam combiner is proposed that completely eliminates the phase inversion subsystem from the nulling interferometer, and instead uses the intrinsic phase shifts in the beam splitters. Simplifying the flight instrument in

this way will be a valuable enhancement of mission reliability. The tighter tolerances on $R = T$ (R being reflection and T being transmission coefficients) required by the self-nulling configuration actually impose no new constraints on the architecture, as

two adaptive nullers must be situated between beam splitters to correct small errors in the coatings.

The new feature is exploiting the natural phase shifts in beam combiners to achieve the 180° phase inversion

necessary for nulling. The advantage over prior art is that an entire subsystem, the field-flipping optics, can be eliminated.

For ultimate simplicity in the flight instrument, one might fabricate coatings to very high tolerances and dispense with the adaptive nullers altogether, with all their moving parts, along with

the field flipper subsystem. A single adaptive nuller upstream of the beam combiner may be required to correct beam train errors (systematic noise), but in some circumstances phase chopping reduces these errors substantially, and there may be ways to further reduce the chop residuals. Though such coatings are beyond the current state of the

art, the mechanical simplicity and robustness of a flight system without field flipper or adaptive nullers would perhaps justify considerable effort on coating fabrication.

This work was done by Eric E. Bloemhof of Caltech for NASA's Jet Propulsion Laboratory. For more information, contact iaoffice@jpl.nasa.gov. NPO-47027

Portable Dew Point Mass Spectrometry System for Real-Time Gas and Moisture Analysis

This system has applications in semiconductor fabrication, industrial gas production, and natural gas refineries.

John F. Kennedy Space Center, Florida

A portable instrument incorporates both mass spectrometry and dew point measurement to provide real-time, quantitative gas measurements of helium, nitrogen, oxygen, argon, and carbon dioxide, along with real-time, quantitative moisture analysis.

The Portable Dew Point Mass Spectrometry (PDP-MS) system comprises a single quadrupole mass spectrometer and a high vacuum system consisting of a turbopump and a diaphragm-backing pump. A capacitive membrane dew point sensor was placed upstream of the MS, but still within the pressure-flow control pneumatic region. Pressure-flow control was achieved with an upstream precision metering valve, a capacitance diaphragm gauge, and a downstream mass flow controller. User configurable LabVIEW software was developed to provide real-time concentration data for the MS, dew

point monitor, and sample delivery system pressure control, pressure and flow monitoring, and recording. The system has been designed to include *in situ*, NIST-traceable calibration.

Certain sample tubing retains sufficient water that even if the sample is dry, the sample tube will desorb water to an amount resulting in moisture concentration errors up to 500 ppm for as long as 10 minutes. It was determined that BeV-A-Line IV was the best sample line to use. As a result of this issue, it is prudent to add a high-level humidity sensor to PDP-MS so such events can be prevented in the future.

This work was done by C. Arkin, Stacey Gillespie, and Christopher Ratzel of ASRC Aerospace Corporation and Mary Whitten of the University of Central Florida for Kennedy Space Center. Further information is contained in a TSP (see page 1). KSC-13316



Maximum Likelihood Time-of-Arrival Estimation of Optical Pulses via Photon-Counting Photodetectors

NASA's Jet Propulsion Laboratory, Pasadena, California

Many optical imaging, ranging, and communications systems rely on the estimation of the arrival time of an optical pulse. Recently, such systems have been increasingly employing photon-counting photodetector technology, which changes the statistics of the observed photocurrent. This requires time-of-arrival estimators to be developed and their performances characterized.

The statistics of the output of an ideal photodetector, which are well

modeled as a Poisson point process, were considered. An analytical model was developed for the mean-square error of the maximum likelihood (ML) estimator, demonstrating two phenomena that cause deviations from the minimum achievable error at low signal power. An approximation was derived to the threshold at which the ML estimator essentially fails to provide better than a random guess of the pulse arrival time. Comparing the analytic

model performance predictions to those obtained via simulations, it was verified that the model accurately predicts the ML performance over all regimes considered.

There is little prior art that attempts to understand the fundamental limitations to time-of-arrival estimation from Poisson statistics. This work establishes both a simple mathematical description of the error behavior, and the associated physical processes that

yield this behavior. Previous work on mean-square error characterization for ML estimators has predominantly focused on additive Gaussian noise.

This work demonstrates that the discrete nature of the Poisson noise process leads to a distinctly different error behavior.

This work was done by Baris I. Erkmen and Bruce E. Moision of Caltech for NASA's Jet Propulsion Laboratory. For more information, contact iaoffice@jpl.nasa.gov. NPO-46857

Handheld White Light Interferometer for Measuring Defect Depth in Windows

The device replaces a refocus microscope for quantification of defects such as scratches and impacts.

John F. Kennedy Space Center, Florida

Accurate quantification of defects (scratches and impacts) is vital to the certification of flight hardware and other critical components. The amount of damage to a particular component contributes to the performance, reliability, and safety of a system, which ultimately affects the success or failure of a mission or test. The launch-commit criteria on a Space Shuttle Orbiter window are governed by the depth of the defects that are identified by a visual inspection. This measurement of a defect is not easy to obtain given the environment, size of the defect, and location of the window(s). The determination of depth has typically been performed by taking a mold impression and measuring the impression with an optical profiling instrument. Another method of obtaining an estimate of the depth is by using a refocus microscope. To use a refocus microscope, the surface of the glass and bottom of the defect are, in turn, brought into focus by the operator. The amount of movement between the two points corresponds to the depth of the defect. The refocus microscope requires a skilled operator and has been proven to be unreliable when used on Orbiter windows. White light interferometry was chosen as a candidate to replace the refocus microscope.

The White Light Interferometer (WLI) was developed to replace the refocus microscope as the instrument used for measuring the depth of defects in Orbiter win-

dows. The WLI consists of a broadband illumination source, interferometer, detector, motion control, displacement sensor, mechanical housing, and support electronics. The illumination source for the WLI is typically a visible light emitting diode (LED) or a near-infrared superluminescent diode (SLD) with power levels of less than a milliwatt. The interferometer is a Michelson configuration consisting of a 1-in. (2.5-cm) cube beam splitter, a 0.5-in. (1.3-cm) optical window as a movable leg (used to closely match the return intensity of the fixed leg from the window), and a mirrored prism to fold the optics into the mechanical housing. The detector may be one of many C-mount CCD (charge-coupled device) cameras. Motion is provided by a commercial nanostepping motor with a serial interface. The displacement sensor is a custom device specifically designed for this application. The mechanical housing and support electronics were designed to integrate the various components into an instrument that could be physically handled by a technician and easily transported.

The WLI is placed over a defect using the video image from the camera. The electronic control is used to reposition the movable mirror. Interference fringes at the surface of the glass are imaged onto the camera (surface position), the mirror is then moved, and interference fringes are formed at various defect site(s). The position of each defect site

can be read from the controller's LCD (liquid crystal display). The difference in these positions from the surface determines the depth of the defect(s).

The device contains an interferometer, and alignment of the optics is critical to the operation of the instrument. Maintenance would consist of the proper alignment of the optics and calibration of the position. The measurement resolution for the instrument was expected to be better than 0.0001 in. (2.5 μm .); the unit has exhibited a resolution on the order of 2 μm . (0.05 μm). This capability is more than adequate for this application, but could be extended with different optics.

While in operation, the WLI displays a continually updated depth measurement on the integrated LCD. The LCD shows displacement information in microns and inches, provides scan speed and direction, mode information, and prompts the operator. Both manual and automatic scans are supported by the electronics; the information is also available from a serial data port. The WLI's use of a video camera allows several people to observe and comment on the defect; consulting/collaboration while using the refocus microscope was not possible.

This work was done by Robert Youngquist, Stephen Simmons, and Robert Cox of Kennedy Space Center. Further information is contained in a TSP (see page 1). KSC-13417



➤ Decomposition Algorithm for Global Reachability on a Time-Varying Graph

This method sequentially solves a series of small problems instead of a single large problem.

NASA's Jet Propulsion Laboratory, Pasadena, California

A decomposition algorithm has been developed for global reachability analysis on a space-time grid. By exploiting the upper block-triangular structure, the planning problem is decomposed into smaller subproblems, which is much more scalable than the original approach.

Recent studies have proposed the use of a hot-air (Montgolfier) balloon for possible exploration of Titan and Venus because these bodies have thick haze or cloud layers that limit the science return from an orbiter, and the atmospheres would provide enough buoyancy for balloons. One of the important questions that needs to be addressed is what surface locations the balloon can reach

from an initial location, and how long it would take. This is referred to as the global reachability problem, where the paths from starting locations to all possible target locations must be computed.

The balloon could be driven with its own actuation, but its actuation capability is fairly limited. It would be more efficient to take advantage of the wind field and "ride" the wind that is much stronger than what the actuator could produce. It is possible to pose the path planning problem as a graph search problem on a directed graph by discretizing the space-time world and the vehicle actuation.

The decomposition algorithm provides reachability analysis of a time-vary-

ing graph. Because the balloon only moves in the positive direction in time, the adjacency matrix of the graph can be represented with an upper block-triangular matrix, and this upper block-triangular structure can be exploited to decompose a large graph search problem. The new approach consumes a much smaller amount of memory, which also helps speed up the overall computation when the computing resource has a limited physical memory compared to the problem size.

This work was done by Yoshiaki Kuwata of Caltech for NASA's Jet Propulsion Laboratory. For more information, contact iaoffice@jpl.nasa.gov. NPO-46941

➤ Autonomous GN&C for Spacecraft Exploration of Comets and Asteroids

An integrated autonomous guidance, navigation, and control capability is developed for enabling precision small-body close-proximity operations and touch-and-go sampling.

NASA's Jet Propulsion Laboratory, Pasadena, California

A spacecraft guidance, navigation, and control (GN&C) system is needed to enable a spacecraft to descend to a surface, take a sample using a touch-and-go (TAG) sampling approach, and then safely ascend. At the time of this reporting, a flyable GN&C system that can accomplish these goals is beyond state of the art. This article describes AutoGNC, which is a GN&C system capable of addressing these goals, which has recently been developed and demonstrated to a maturity TRL-5-plus.

The AutoGNC solution matures and integrates two previously existing JPL capabilities into a single unified GN&C system. The two capabilities are AutoNAV and G-REX. AutoNAV is JPL's current flight navigation system, and is fairly mature with respect to flybys and rendezvous with small bodies, but is lacking capability for close surface proximity operations, sampling,

and contact. G-REX is a suite of low-TRL algorithms and capabilities that enables spacecraft operations in close surface proximity and for performing sampling/contact. The development and integration of AutoNAV and G-REX components into AutoGNC provides a single, unified GN&C capability for addressing the autonomy, close-proximity, and sampling/contact aspects of small-body sample return missions.

AutoGNC is an integrated capability comprising elements that were developed separately. The main algorithms and component capabilities that have been matured and integrated are autonomy for near-surface operations, terrain-relative navigation (TRN), real-time image-based feedback guidance and control, and six degrees of freedom (6DOF) control of the TAG sampling event.

Autonomy is achieved based on an AutoGNC Executive written in Virtual Ma-

chine Language (VML) incorporating high-level control, data management, and fault protection. In descending to the surface, the AutoGNC system uses camera images to determine its position and velocity relative to the terrain. This capability for TRN leverages native capabilities of the original AutoNAV system, but required advancements that integrate the separate capabilities for shape modeling, state estimation, image rendering, defining a database of onboard maps, and performing real-time landmark recognition against the stored maps.

The ability to use images to guide the spacecraft requires the capability for image-based feedback control. In AutoGNC, navigation estimates are fed into an onboard guidance and control system that keeps the spacecraft guided along a desired path, as it descends towards its targeted landing or sampling

site. Once near the site, AutoGNC achieves a prescribed guidance condition for TAG sampling (position/orientation, velocity), and a prescribed force profile on the sampling end-effector. A dedicated 6DOF TAG control then implements the ascent burn while recovering from sampling disturbances and induced attitude rates. The control also minimizes structural interactions with flexible solar panels and disallows any

part of the spacecraft from making contact with the ground (other than the intended end-effector).

This work was done by John M. Carson, Nickolaos Mastrodemos, David M. Myers, Behcet Acikmese, James C. Blackmore, Dhemitrio Boussalis, Joseph E. Riedel, Simon Nolet, Johnny T. Chang, Milan Mandic, Laureano (Al) Cangahuala, Stephen B. Broschart, David S. Bayard, Andrew T. Vaughan, Tseng-Chan M. Wang,

and Robert A. Werner of Caltech; Christopher A. Grasso of Blue Sun Enterprises; and Gaskell W. Robert of the Planetary Science Institute for NASA's Jet Propulsion Laboratory. Further information is contained in a TSP (see page 1).

The software used in this innovation is available for commercial licensing. Please contact Daniel Broderick of the California Institute of Technology at danielb@caltech.edu. Refer to NPO-47250.

➤ Efficient Web Services Policy Combination

This algorithm serves as the basis for reliable, fast, and automatic network communications.

NASA's Jet Propulsion Laboratory, Pasadena, California

Large-scale Web security systems usually involve cooperation between domains with non-identical policies. The network management and Web communication software used by the different organizations presents a stumbling block. Many of the tools used by the various divisions do not have the ability to communicate network management data with each other. At best, this means that manual human intervention into the communication protocols used at various network routers and endpoints is required. Developing practical, sound, and automated ways to compose policies to bridge these differences is a long-standing problem. One of the key subtleties is the need to deal with inconsistencies and defaults where one organization proposes a rule on a particular feature, and another has a different rule or expresses no rule. A general approach is to assign priorities to rules and observe the rules with the highest priorities when there are conflicts.

The present methods have inherent inefficiency, which heavily restrict their practical applications. A new, efficient algorithm combines policies utilized for

Web services. The method is based on an algorithm that allows an automatic and scalable composition of security policies between multiple organizations. It is based on defeasible policy composition, a promising approach for finding conflicts and resolving priorities between rules.

In the general case, policy negotiation is an intractable problem. A promising method, suggested in the literature, is when policies are represented in defeasible logic, and composition is based on rules for non-monotonic inference. In this system, policy writers construct metapolicies describing both the policy that they wish to enforce and annotations describing their composition preferences. These annotations can indicate whether certain policy assertions are required by the policy writer or, if not, under what circumstances the policy writer is willing to compromise and allow other assertions to take precedence. Meta-policies are specified in defeasible logic, a computationally efficient non-monotonic logic developed to model human reasoning.

One drawback of this method is that at one point the algorithm starts an ex-

haustive search of all subsets of the set of conclusions of a defeasible theory. Although the propositional defeasible logic has linear complexity, the set of conclusions here may be large, especially in real-life practical cases. This phenomenon leads to an inefficient exponential explosion of complexity.

The current process of getting a Web security policy from combination of two meta-policies consists of two steps. The first is generating a new meta-policy that is a composition of the input meta-policies, and the second is mapping the meta-policy onto a security policy. The new algorithm avoids the exhaustive search in the current algorithm, and provides a security policy that matches all requirements of the involved meta-policies.

This work was done by Farrokh Vatan and Joseph G. Harman of Caltech for NASA's Jet Propulsion Laboratory. Further information is contained in a TSP (see page 1).

The software used in this innovation is available for commercial licensing. Please contact Daniel Broderick of the California Institute of Technology at danielb@caltech.edu. Refer to NPO-47279.

➤ Using CTX Image Features to Predict HiRISE-Equivalent Rock Density

NASA's Jet Propulsion Laboratory, Pasadena, California

Methods have been developed to quantitatively assess rock hazards at candidate landing sites with the aid of images from the HiRISE camera onboard NASA's Mars Reconnaissance Orbiter. HiRISE is able to resolve rocks as small as 1-m in di-

ameter. Some sites of interest do not have adequate coverage with the highest resolution sensors and there is a need to infer relevant information (like site safety or underlying geomorphology). The proposed approach would make it possible

to obtain rock density estimates at a level close to or equal to those obtained from high-resolution sensors where individual rocks are discernable.

The low-resolution data considered here are CTX images, which have a

lower resolution than HiRISE images but have a broader span. An important characteristic of CTX and HiRISE images is that they are captured concurrently. Thus, there is a natural pairing between the two data sets.

Bayesian Networks (BNs) are used to graphically model the statistical relationship between rock density estimated from HiRISE images and features extracted from CTX images. Gray Level Co-occurrence Matrix (GLCM) features

are used to model the texture in CTX images. The statistical relationship among CTX image features, geomorphology, and rock density is learned by incorporating rock counts from HiRISE images and geomorphic information provided by scientists corresponding to the landing site. The trained BN is then used to infer rock density directly from CTX image features even in the absence of higher resolution images like HiRISE.

This work was done by Navid Serrano and Andres Huertas of Caltech and Patrick McGuire, David Mayer, and Raymond Arvidson of Washington University in Saint Louis for NASA's Jet Propulsion Laboratory. For more information, contact iaoffice@jpl.nasa.gov.

The software used in this innovation is available for commercial licensing. Please contact Daniel Broderick of the California Institute of Technology at danielb@caltech.edu. Refer to NPO-46989.



Isolation of the *Paenibacillus phoenicis*, a Spore-Forming Bacterium

NASA's Jet Propulsion Laboratory, Pasadena, California

A microorganism was isolated from the surfaces of the cleanroom facility in which the Phoenix lander was assembled. The isolated bacterial strain was subjected to a comprehensive polyphasic analysis to characterize its taxonomic position. Both phenotypic and phylogenetic analyses clearly indicate that this isolate belongs to the genus *Paenibacillus* and represents a novel species.

Bacillus spores have been utilized to assess the degree and level of microbiological contamination on spacecraft and

their associated spacecraft assembly facilities. Spores of *Bacillus* species are of particular concern to planetary protection due to the extreme resistance of some members of the genus to space environmental conditions such as UV and gamma radiation, vacuum, oxidation, and temperature fluctuation. These resistive spore phenotypes have enhanced potential for transfer, and subsequent proliferation, of terrestrial microbes on another solar body. Due to decreased nutrient conditions within spacecraft as-

sembly facility clean rooms, the vegetative cells of *Bacillus* species and other spore-forming *Paenibacillus* species are induced to sporulate, thereby enhancing their survivability of bioreduction

This work was done by James N. Benardini, Parag A. Vaishampayan, and Kasthuri J. Venkateswaran of Caltech; Shariff Osman of Lawrence Livermore National Laboratory; and Masataka Satomi of the Japanese National Research Institute for NASA's Jet Propulsion Laboratory. For more information, contact iaoffice@jpl.nasa.gov. NPO-47232

Monolithically Integrated, Mechanically Resilient Carbon-Based Probes for Scanning Probe Microscopy

These probes can be used in medical applications for bacteria or protein imaging.

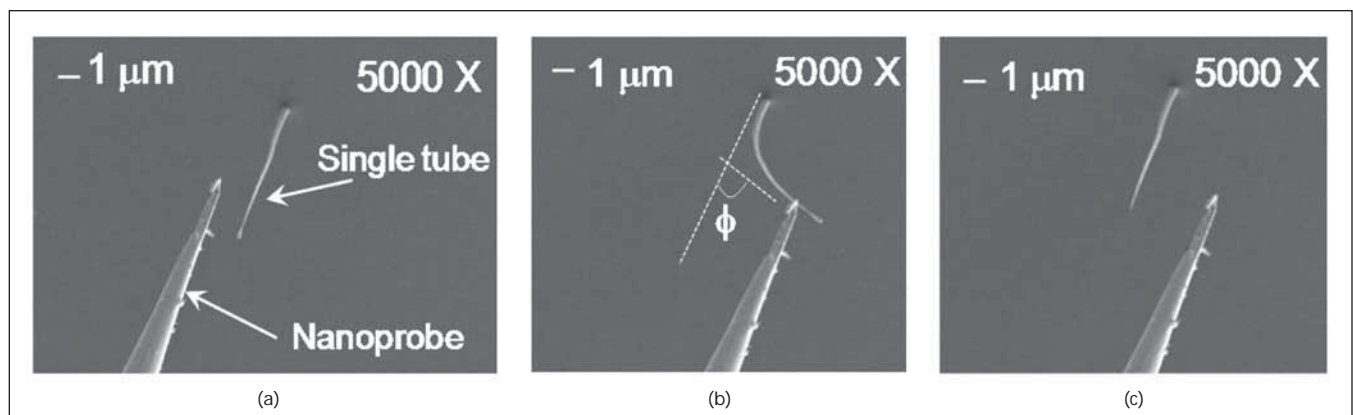
NASA's Jet Propulsion Laboratory, Pasadena, California

Scanning probe microscopy (SPM) is an important tool for performing measurements at the nanoscale in imaging bacteria or proteins in biology, as well as in the electronics industry. An essential element of SPM is a sharp, stable tip that possesses a small radius of curvature to enhance spatial resolution. Existing techniques for forming such tips are not ideal. High-aspect-ratio, monolithically integrated, as-grown carbon

nanofibers (CNFs) have been formed that show promise for SPM applications by overcoming the limitations present in wet chemical and separate substrate etching processes.

The CNFs of this innovation have been synthesized in a load-lock-based DC PECVD (plasma-enhanced chemical vapor deposition) growth chamber, where the CNF growth was done on Si substrate with high-purity acetylene

(C_2H_2) and ammonia (NH_3) at 700 °C. The ratio of $C_2H_2:NH_3 = [1:4]$, which has been determined to minimize the amount of amorphous carbon on the substrate during growth. When the desired growth pressure was attained (3–15 Torr), a DC glow discharge was ignited, and growth was continued for a fixed duration. The PECVD growth parameters, such as growth pressure, catalyst thickness, and plasma power, were var-



The CNFs Are Mechanically Resilient and should enable enhanced cycling longevity for NEMS applications: (a) A nanoprobe was in close proximity to a single CNF. (b) The probe was mechanically manipulated so that it deflected the CNF to the right. The CNF accommodated large bending angle without fracture or delamination, with $\phi \approx 70^\circ$ over tens of cycles. (c) The CNF returned elastically to its initial position after the probe was removed.

ied to see their impact on the physical characteristics of the CNFs (e.g., diameter and length).

The mechanical characteristics of the CNFs were measured in a custom-built *in-situ* mechanical deformation instrument, the SEMentor, comprising a scanning electron microscope (SEM) and the nanoindenter. This instrument has generally been used to explore uniaxial deformation and defect evolution in individual, metallic pillars formed by using the focused-ion-beam (FIB), for example.

Bending tests were performed with a nanoprobe that deflected an individual CNF, and provided insight into their mechanical resilience in shear. *In-situ* electrical measurements were then conducted on individual, as-grown CNFs using a nanomanipulator probe stage mounted inside an SEM (FEI Quanta 200F) that was equipped with an electrical feed-through. Tungsten probes were used to make the two-terminal electrical

measurements of individual, vertically oriented, as-grown CNFs with an HP4156C parameter analyzer.

For SPM applications, stress concentrators may exist at the CNF-to-substrate interface, as well as within the body. *In-situ* uniaxial compression tests were performed on arrays of CNFs inside the SEMentor, which provided some insight into the nature of the mechanical bond between the CNF and substrate. A Berkovich tip, which is a pyramidal, shallow-angled tip, was used to indent the forest of CNFs. The SEM image taken after indentation revealed that the CNFs fractured within the tube body rather than at the CNF-to-substrate interface, where a fracture angle $\alpha_f \approx 25^\circ$ – 35° (relative to the CNF or central axis) was computed.

The significance of α_f was correlated to the structural characteristics of the CNFs, which were deciphered from transmission electron microscopy (TEM) that was performed with FEI Tecnai-F20 Scanning

–(S) TEM, with a field emission source of 200 kV. The TEM analysis of the mechanically transferred CNFs grown directly on Si revealed a herringbone structure where the graphite basal planes were inclined to the central axis at a cone angle α , where $\alpha \approx 30^\circ$. Since α_f and α did not differ appreciably, the nanomechanical measurements performed in the SEMentor confirm that the CNFs sheared from within the basal planes of the CNFs, indicating that the adhesion of the CNFs to the substrate was very strong. In addition, the image in the figure shows the CNFs can tolerate a large degree of mechanical strain where bending angles ϕ as large as 70° could be accommodated elastically, confirming the promise such carbon-based nanostructures have for SPM applications.

This work was done by Anupama B. Kaul, Krikor G. Megerian, Andrew T. Jennings, and Julia R. Greer of Caltech for NASA's Jet Propulsion Laboratory. For more information, contact iaoffice@jpl.nasa.gov. NPO-47185

Cell Radiation Experiment System

Cells can be irradiated under conditions that approximate those in living tissues.

Lyndon B. Johnson Space Center, Houston, Texas

The cell radiation experiment system (CRES) is a perfused-cell culture apparatus, within which cells from humans or other animals can (1) be maintained in homeostasis while (2) being exposed to ionizing radiation during controlled intervals and (3) being monitored to determine the effects of radiation and the repair of radiation damage. The CRES can be used, for example, to determine effects of drug, radiation, and combined drug and radiation treatments on both normal and tumor cells. The CRES can also be used to analyze the effects of radiosensitive or radioprotectant drugs on cells subjected to radiation. The knowledge gained by use of the CRES is expected to contribute to the development of better cancer treatments and of better protection for astronauts, medical-equipment operators, and nuclear-power-plant workers, and others exposed frequently to ionizing radiation.

Traditionally, experiments to determine the effects of ionizing radiation on cells involved (1) culturing the cells in test tubes, Petri dishes, or culture flasks; (2) removing the cells from the cultures and exposing them to radia-

tion; and (3) reculturing the cells to enable the cells to attempt to repair the radiation damage and continue to grow. The great disadvantage of the traditional approach is that cells are subjected to a succession of environments that differ radically from the precisely controlled natural environment in a human or other animal body; the effects of the succession of nonlifelike environments can alter the subtle effects of radiation damage mechanisms and intracellular repair processes, thereby introducing uncertainty into interpretation of experimental observations. By maintaining more nearly lifelike conditions, the CRES can increase the accuracy of, and confidence in, experimental observations.

The CRES (see figure) includes one or more cell-culture chambers equipped with a very thin, impermeable Mylar (or equivalent polyethylene terephthalate) membrane at one end, described in more detail below. At the opposite end of each culture chamber there is a perfusion chamber separated from a culture chamber by a permeable membrane. Through this membrane, waste and nutrients are exchanged between the cul-

ture and perfusion chambers. A circulation subsystem that includes fluid reservoirs, conduits, valves, pumps, and automated process controls provides for the slow perfusion of the nutrient medium used to culture the cells.

The system includes a source of ionizing radiation in a shielded enclosure with motor-driven shutters that are used to effect timed, selective irradiation of the cell-culture chamber(s). A process-control module exerts overall control over the circulation subsystem and other subsystems to regulate such parameters as the temperature, the rate of circulation of fresh nutrient medium, the pH of the medium, and radiation doses via the shutters. Another subsystem monitors the metabolic rates of cells by measuring ultraviolet fluorescence from the cells, the pH of the medium, and/or the concentrations of O₂ and CO₂. Still another subsystem under control by the process-control module can be made to introduce a fixative substance to preserve the cell cultures for subsequent analysis. The impermeable front membrane is thin enough to allow the ionizing radiation to pass through. Before installation, the inner face of this

membrane is subjected to a special oxygen etch to enable epithelial or other anchor-dependent cells to attach themselves. As a result, a monolayer of cells

grows on this membrane and, by virtue of the precision with which their location is thus known, radiation dosimetry can be quite accurate.

This work was done by Dennis R. Morrison of Johnson Space Center. Further information is contained in a TSP (see page 1). MSC-23060-1



Process To Produce Iron Nanoparticle Lunar Dust Simulant Composite

A document discusses a method for producing nanophase iron lunar dust composite simulant by heating a mixture of carbon black and current lunar simulant types (mixed oxide including iron oxide) at a high temperature to reduce ionic iron into elemental iron. The product is a chemically modified lunar simulant that can be attracted by a magnet, and has a surface layer with an iron concentration that is increased during the reaction. The iron was found to be α -iron and Fe_3O_4 nanoparticles. The simulant produced with this method contains iron nanoparticles not available previously, and they are stable in ambient air. These nanoparticles can be mass-produced simply.

This work was done by Ching-cheh Hung and Jeremiah McNatt of Glenn Research Center.

Inquiries concerning rights for the commercial use of this invention should be addressed to NASA Glenn Research Center, Innovative Partnerships Office, Attn: Steve Fedor, Mail Stop 4-8, 21000 Brookpark Road, Cleveland, Ohio 44135. Refer to LEW-18496-1.

Inversion Method for Early Detection of ARES-1 Case Breach Failure

A document describes research into the problem of detecting a case breach formation at an early stage of a rocket flight. An inversion algorithm for case breach allocation is proposed and analyzed. It is shown how the case breach can be allocated at an early stage of its development by using the rocket sensor data and the output data from the control block of the rocket navigation system. The results are simulated with MATLAB/Simulink software. The efficiency of an inversion algorithm for a case breach location is discussed.

The research was devoted to the analysis of the ARES-1 flight during the first 120 seconds after the launch and early prediction of case breach failure. During this time, the rocket is propelled by its first-stage Solid Rocket Booster (SRB). If a breach appears in SRB case, the gases escaping through it will produce the (side) thrust directed perpendicular to the rocket axis. The side thrust creates a

torque influencing the rocket attitude. The ARES-1 control system will compensate for the side thrust until it reaches some critical value, after which the flight will be uncontrollable. The objective of this work was to obtain the start time of case breach development and its location using the rocket inertial navigation sensors and GNC data.

The algorithm was effective for the detection and location of a breach in an SRB field joint at an early stage of its development.

This work was done by Ryan M. Mackey and Igor K. Kulikov of Caltech and Anupa Bajwa, Peter Berg, and Vadim Smelyanskiy of Ames Research Center for NASA's Jet Propulsion Laboratory. Further information is contained in a TSP (see page 1).

The software used in this innovation is available for commercial licensing. Please contact Daniel Broderick of the California Institute of Technology at danielb@caltech.edu. Refer to NPO-47285.

Use of ILTV Control Laws for LaNCETS Flight Research

A report discusses the Lift and Nozzle Change Effects on Tail Shock (LaNCETS) test to investigate the effects of lift distribution and nozzle-area ratio changes on tail shock strength of an F-15 aircraft. Specific research objectives are to obtain in-flight shock strength for multiple combinations of nozzle-area ratio and lift distribution; compare results with pre-flight prediction tools; and update predictive tools with flight results. The objectives are to ensure adequate aircraft stability for the changes in lift distribution and plume shape, and ensure manageable transient from engaging and disengaging the ILTV research control laws. In order to change the lift distribution and plume shape of the F-15 aircraft, a decade-old Inner Loop Thrust Vectoring (ILTV) research control law was used. Flight envelope expansion was performed for the test configuration and flight conditions prior to the probing test points.

The approach for achieving the research objectives was to utilize the unique capabilities of NASA's NF-15B-837 aircraft to allow the adjustment of the nozzle-area ratio and/or canard positions by engaging the ILTV research

control laws. The ILTV control laws provide the ability to add trim command biases to canard positions, nozzle area ratios, and thrust vectoring through the use of datasets. Datasets consist of programmed test inputs (PTIs) that define "trims" to change the nozzle-area ratio and/or canard positions. The trims are applied as increments to the normally commanded positions.

A LaNCETS non-linear, six-degrees-of-freedom simulation capable of real-time pilot-in-the-loop, hardware-in-the-loop, and non-real-time batch support was developed and validated. Prior to first flight, extensive simulation analyses were performed to show adequate stability margins with the changes in lift distribution and plume shape. Additionally, engagement/disengagement transient analysis was also performed to show manageable transients.

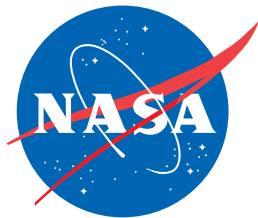
This work was done by Cheng Moua of Dryden Flight Research Center. Further information is contained in a TSP (see page 1). DRC-009-039

Evaluating Descent and Ascent Trajectories Near Non-Spherical Bodies

Spacecraft landing on small bodies pass through regions where conventional gravitation formulations using exterior spherical harmonics are inaccurate. An investigation shows that a formulation using interior solid spherical harmonics might be satisfactory. Interior spherical harmonic expansions are usable inside an imaginary, empty sphere. For this application, such a sphere could be positioned in empty space above the intended landing site and rotating with the body. When the spacecraft is inside this sphere, the interior harmonic expansion would be used instead of the conventional, exterior harmonic expansion.

Coefficients can be determined by a least-squares fit to gravitation measurements synthesized from conventional formulations. Due to their unfamiliarity, recurrences for interior, as well as exterior, expansions are derived. Hotine's technique for partial derivatives of exterior spherical harmonics is extended to interior harmonics.

This work was done by Robert A. Werner of Caltech for NASA's Jet Propulsion Laboratory. Further information is contained in a TSP (see page 1). NPO-46697



National Aeronautics and
Space Administration